minerals

MDPI

Review

Thermochronology of Alkali Feldspar and Muscovite at T > 150 °C Using the $^{40}Ar/^{39}Ar$ Method: A Review

Richard A. Spikings [1,*] and Daniil V. Popov [2]

[1] Department of Earth Sciences, University of Geneva, 1205 Geneva, Switzerland
[2] School of Environment, Earth and Ecosystem Sciences, The Open University, Walton Hall, Milton Keynes MK7 6AA, UK; d.vs.popov@gmail.com
* Correspondence: richard.spikings@unige.ch

Abstract: The $^{40}Ar/^{39}Ar$ method applied to K-feldspars and muscovite has been often used to construct continuous thermal history paths between ~150–600 °C, which are usually applied to structural and tectonic questions in many varied geological settings. However, other authors contest the use of $^{40}Ar/^{39}Ar$ thermochronology because they argue that the assumptions are rarely valid. Here we review and evaluate the key assumptions, which are that (i) ^{40}Ar is dominantly redistributed in K-feldspars and muscovite by thermally-driven volume diffusion, and (ii) laboratory experiments (high temperatures and short time scales) can accurately recover intrinsic diffusion parameters that apply to geological settings (lower temperatures over longer time scales). Studies do not entirely negate the application of diffusion theory to recover thermal histories, although they reveal the paramount importance of first accounting for fluid interaction and secondary reaction products via a detailed textural study of single crystals. Furthermore, an expanding database of experimental evidence shows that laboratory step-heating can induce structural and textural changes, and thus extreme caution must be made when extrapolating laboratory derived rate loss constants to the geological past. We conclude with a set of recommendations that include minimum sample characterisation prior to degassing, an assessment of mineralogical transformations during degassing and the use of in situ dating.

Keywords: $^{40}Ar/^{39}Ar$; thermochronology; diffusion; K-feldspar; muscovite; in situ dating

check for updates

Citation: Spikings, R.A.; Popov, D.V. Thermochronology of Alkali Feldspar and Muscovite at T > 150 °C Using the $^{40}Ar/^{39}Ar$ Method: A Review. *Minerals* **2021**, *11*, 1025. https://doi.org/10.3390/min11091025

Academic Editor: Koen De Jong

Received: 19 August 2021
Accepted: 17 September 2021
Published: 21 September 2021

1. Introduction

Many geological processes alter the temperature of minerals, and hence an accurate, quantitative determination of that change can be used to study a wide range of phenomena, such as metamorphism, deformation, exhumation and burial. The recovery of time(t)-Temperature(T) paths from isotopic data exploits the thermally driven diffusive loss of isotopes that form by spontaneous radioactive decay, which leads to several key assumptions that form the basis of most thermochronological methods. Arguably the most important assumption is that thermally activated volume diffusion has been the dominant influence on the redistribution and loss of daughter isotopes from minerals. The diffusive process either results in the redistribution of isotopes towards a mineral or subgrain boundary, or recrystallizes lattice defects (e.g., fission tracks). However, isolating the effects of temperature on isotope mobility from other phenomena such as fluid induced mineral reactions and structural transformations (e.g., [1–3]) is challenging. The second key assumption is that laboratory diffusion experiments at high temperatures replicate the physical mechanisms that occur with natural rates of cooling and heating over geological timescales. Here we review published research on whether these assumptions hold for the alkali feldspar and muscovite $^{40}Ar/^{39}Ar$ thermochronological methods, where some studies have suggested these can recover thermal histories at ~150–350 °C (e.g., [4–6]) and ~300–600 °C [7–11], respectively. Many studies have questioned the applicability of these

methods and argued that the migration of Ar isotopes in alkali feldspar and muscovite is governed by different mechanisms in the laboratory and during the geological past, and thus cannot be described using a single set of diffusion parameters [2,3,12–17]. Only a small percentage of thermochronological studies have developed and applied thermochronometers that can generate continuous t-T paths at T > 150 °C, while the most frequently used (fission track and (U-Th/He)) are sensitive to T < 150 °C. Therefore, we aim to provide ideas to stimulate further research into how to test the aforementioned key assumptions, and perhaps identify intra-grain regions where natural argon diffusion profiles may have been preserved and can be recovered intact.

2. Recovering Continuous Thermal History Information Using the $^{40}Ar/^{39}Ar$ Method

Some studies of Ar in K-feldspars and muscovite suggest that their Ar isotopic compositions can be exploited to recover accurate, continuous t-T paths at T ~150–350 °C (e.g., [4–6]) and ~300–600 °C [7–11], respectively (Figure 1), in some cases. Following Fick's law of diffusion, thermochronological methods utilise a mathematical description that relates properties of the host structure (activation energy of diffusion, E_a, and absolute diffusivity, D_0), cooling rate, the geometry and size of the diffusion domain(s) (i.e., length scale(s) for diffusion) and t-T history with degree of daughter isotope loss (e.g., [4]). Therefore, the application of thermochronology to any particular mineral and decay scheme is completely dependent on whether or not the user (i) can demonstrate that the daughter isotope has been lost by diffusion, both in the laboratory and in nature, (ii) can show that laboratory (high-temperature) and natural (low-temperature) diffusion followed the same Arrhenius relationship, (iii) has a knowledge of the intrinsic diffusion properties of the mineral phase, and (iv) can determine how many length scales exist within a single or bulk collection of crystals, and how these different length scales (domains) interact. The user must also understand how the displacing daughter isotope is redistributed once it reaches the host mineral surface. Is the mineral boundary open to the extent that it can be accurately approximated to have a zero concentration of the diffusing isotope, or not (e.g., [18–20])?

Two major approaches have been used to extract Ar isotope data for the purpose of thermochronology. The first approach is step-heating analysis, where one or several grains of either alkali feldspar or muscovite are degassed in a resistance furnace attached to a thermocouple (larger volume fractions), or using an infra-red laser coupled to a pyrometer (lower volume samples). Heating schedules are frequently cycled, such that individual or sequences of heating steps are repeated with an overall increase in temperature. The two distinct sources of information obtained from a step-heating experiment are the $^{40}Ar/^{39}Ar$ age spectrum (Figure 1A,B), which is often used as a proxy for intra-grain distribution of radiogenic Ar, and the Arrhenius plot (Figure 1C,D), which characterises the combined effect of diffusion domain(s) properties on Ar release. A log(r/r0) plot shows the effective diffusion length of domains that degas during a given heating step (Figure 1E,F; r0 is considered to be the effective diffusion length during the first heating step), assuming that the non-linearity in the Arrhenius plot is only a consequence of the presence of multiple intra-grain diffusion domains. To extract t-T information from these data, the user must (i) determine the number of diffusion domains and their respective diffusion properties (E_a and D_0), (ii) determine the relative sizes of the domains and their contribution to the volume of gas released during each heating step, and (iii) invert or forward model the data to seek plausible t-T paths (Figure 1G,H). This process is referred to as Multi-Diffusion Domain (MDD) modelling, and the inversion theory was developed by Lovera et al. (1989) [4] and Lovera and Richter (1991) [5], while several authors have written code to perform this task (e.g., [21–23]). The second approach is to use in situ $^{40}Ar/^{39}Ar$ analysis, where Ar isotopic compositions are measured in polished grains by ablation using a UV laser to characterise intra-grain $^{40}Ar/^{39}Ar$ date variations (e.g., [6,16,24,25]). Potential t-T paths can be generated by forward modelling using software such as Diffarg(P) and choosing an appropriate set of diffusion parameters (Figure 2A; [8,26,27]). The semi-closed nature

of boundaries for Ar loss could be accounted for by changing the boundary conditions in Diffarg(P), or adopting a more sophisticated approach, such as those used by Baxter (2003) [28] and Popov and Spikings (this volume) [20]. The potential presence of defects such as nanotunnels that may facilitate diffusive Ar loss [29,30] could be accounted for by applying a model of multi-path transport (e.g., [31]).

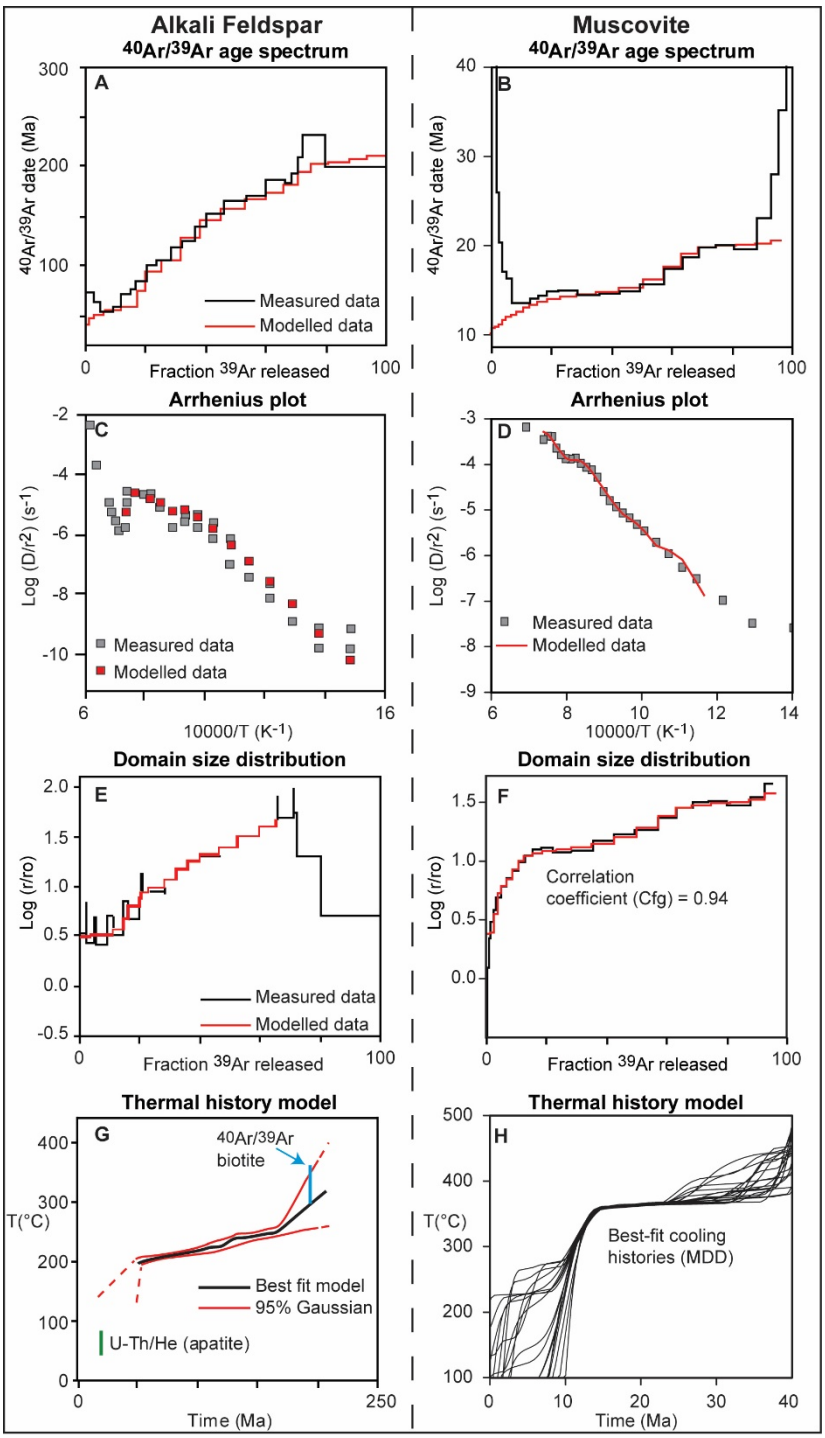

Figure 1. Multi-domain diffusion modeling of argon isotope data acquired from alkali feldspar [22] and muscovite [32]. (**A**,**B**) The age spectrum (distribution of radiogenic ^{40}Ar relative to reactor produced $^{39}Ar_K$), which is interpreted to be the function of the t-T history of the analysed grain(s). (**C**,**D**) The Arrhenius plot, which is a function of the heating schedule and the grain(s) structure. The activation energy (268 kJ/mol) used to construct the Arrhenius plot for the muscovite is taken from

hydrothermal diffusion experiments performed by Harrison et al. (2009) [7]. (**E**,**F**) The "log(r/ro)" plot [33], which measures deviations from linearity in Arrhenian space, and is a function of the structure of the grain(s), and their t-T history, and is independent of the heating schedule, and (**G**,**H**) modeled t-T solutions that fit the measured data. The inversion process assumes that Ar is redistributed and lost from the grains(s) by volume diffusion from non-interacting domains of variable size, each of which is bounded by fast pathways to an infinite reservoir. Harrison and Lovera (2014) [32] report that the close correlation between the age and Log (r/ro) spectra (measured by the Cfg parameter where a value of 1 indicates perfect correlation) is evidence that volume diffusion in the laboratory mimics Ar loss in nature, and thus that the t-T models are accurate.

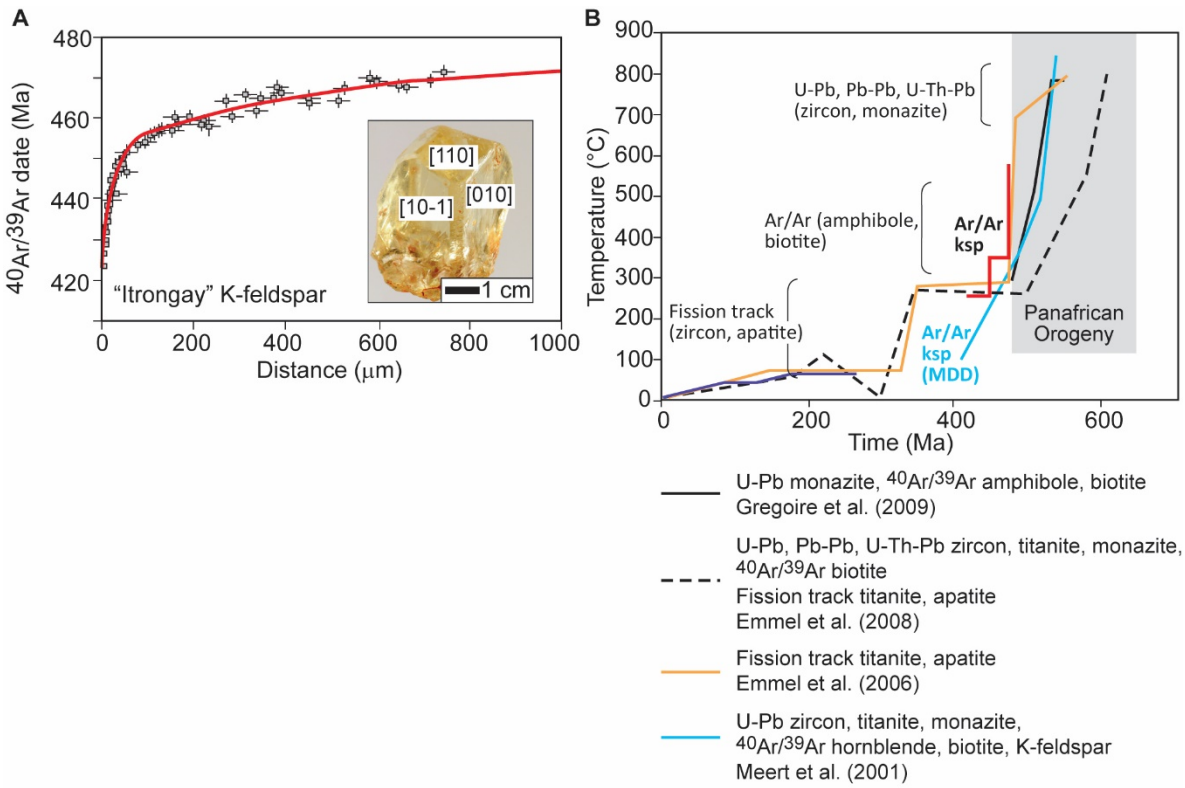

Figure 2. (**A**) Composite in situ $^{40}Ar/^{39}Ar$ date profile obtained from depth profiles from [010] and [110] crystal faces of gem quality alkali feldspar from Itrongay, Madagascar, with uncertainties of 1-sigma. Data were obtained by UV laser ablation, and are from Flude et al. (2014) [6]. (**B**) Flude et al. (2014) [6] interpret the data to reflect diffusive ^{40}Ar loss through a single length scale with a distance of at least 1cm, and derive a possible t-T solution (in red) using diffusion parameters that were previously obtained by Wartho et al. (1999) [34]. Flude et al. (2014) [6] suggest the accuracy of their t-T solution is supported by similarities with other t-T paths (shown) that have been derived for southern Madagascar using the U-Pb, $^{40}Ar/^{39}Ar$ and fission track methods.

2.1. Alkali Feldspar

Many studies have generated continuous t-T paths by applying MDD modeling to $^{40}Ar/^{39}Ar$ data acquired by step-heating of K-feldspars to investigate a wide range of tectonic processes. These include mountain and plateau building processes (e.g., [35–38]), the post-orogenic histories of cratons (e.g., [39,40]), core complex formation (e.g., [41,42]) and continental rifts (e.g., [43]). The use of step-heating $^{40}Ar/^{39}Ar$ analysis of K-feldspar for thermochronology is supported by Lovera et al. (1996, 2002) [44,45], who suggested that correlation between inflexions observed in the age spectra (which they interpret to reflect Ar accumulation and re-distribution in the geologic past) and the log (r/r0) plots (which they interpret to reflect variations in sizes of actively degassing domains during laboratory analysis) is evidence that diffusion mechanisms and diffusion domain boundaries in nature

are the same as those exploited during laboratory degassing. To quantify this, Lovera et al. (2002) [45] defined a cross-correlation coefficient (C_{fg}; Figure 1F), which showed a high correlation in >70% of studied K-feldspars. This led them to conclude that MDD modelling correctly simulates the natural diffusion history, and thus can be used to invert t-T paths in most samples (e.g., [32]). Lovera et al. (1993) [46] performed a double-irradiation experiment to test if hypothetical intra-grain diffusion domains remain stable over the course of laboratory analysis, in which the same alkali feldspars underwent step-wise heating at temperatures between 450–850 °C, before and subsequent to a 2nd irradiation step. Both step-heating experiments yielded almost identical Arrhenius plots between 450–850 °C, which led them to conclude that departures from linearity in Arrhenian space are not due to modifications of texture or structure, but are due to the exhaustion of Ar from domains with variable length scales.

More recently, in situ $^{40}Ar/^{39}Ar$ dating has been applied to alkali feldspars to test the assumption that Ar redistribution in this mineral can be dominated by volume diffusion. Flude et al. (2014) [6] recovered $^{40}Ar/^{39}Ar$ date profiles over distances of ~1cm (UV ablation) in single crystals of orthoclase (Itrongay, Madagascar). These variations were attributed to volume diffusion through a single length scale (Figure 2A), partly because they could be reproduced by forward modelling using diffusion parameters determined for other crystals from the same locality [34] and the resulting t-T path is similar to the regional thermal history constrained by other authors using the U-Pb, $^{40}Ar/^{39}Ar$ and fission track methods (Figure 2B).

2.2. Muscovite

Some in situ $^{40}Ar/^{39}Ar$ dates in white micas have been reported as diffusion gradients (e.g., [25,47,48]), and staircase-shaped $^{40}Ar/^{39}Ar$ age spectra obtained by step-heating have been interpreted in some cases to reflect diffusive loss of Ar through the geologic past [49,50]. Harrison et al. (2009) [7] performed hydrothermal diffusion experiments and proposed that small flakes of muscovite can retain the Ar diffusion boundaries and length scales that define their natural retentivity during *in-vacuo* step-heating (see also [45]), and thus they can be used to reconstruct continuous t-T paths. The same authors report E_A and D_0 diffusion data for muscovite, which have been used by subsequent workers to derive thermal histories. Heizler and Harrison (2009) [51] expanded on that work and report that diffusion domains within muscovite have length scales that vary between $\leq$125 and 1 micrometers, which provides clues about the nature of the domains, although their identification remains elusive, if they exist. Forster et al. (2011) [52] corroborate Harrison et al. (2009) [7] and report that laboratory furnace extraction of Ar from multi-grain, detrital white mica (Indus Basin) reveals natural diffusional loss from two length scales. Harrison and Lovera (2014) [32] applied MDD modelling to $^{40}Ar/^{39}Ar$ data from muscovite from the Main Central Thrust (Figure 1), Himalayas, to generate t-T solutions that are consistent with a large regional dataset, perhaps validating the use of muscovite as a thermochronometer in their rocks, and the presence of multiple, intra-grain diffusion length scales. Forster and Lister (2014) [9] claim that diffusion profiles can be extracted from multi-grain, muscovite-phengite mixtures in high-pressure metamorphic rocks using in-vacuo furnace heating. More recently, Uunk et al. (2018) [15] utilised the heterogeneity in total fusion dates of single white mica crystals from retrogressed blueschists to identify some hand specimens where the grains were semi-closed to Ar loss, and other hand specimens that preserved diffusion profiles in white mica, thereby suggesting that diffusion profiles can exist in certain circumstances. Long et al. (2018, Basin and Range) [10] and Gonzales and Baldwin (2019, Baja California) [11] applied furnace step-heating and MDD modelling to high-pressure phengite and muscovite, respectively, and derived continuous t-T histories. Well-defined age gradients and highly correlated age spectra and log (r/r0) plots led these authors to conclude that their t-T solutions are accurate.

Summarising, some studies have derived t-T solutions from suspected diffusion profiles in muscovite by either (i) testing a restricted number of forward t-T models of bulk

grains assuming a single length scale and using the MatLab^{TM} code, Diffarg (e.g., [15]), or (ii) inversion using MDD modelling (e.g., [7,10,11,32]). Only four studies have constrained t-T solutions using inversion (i.e., testing 10^3–10^4 potential t-T solutions), while permitting the possible existence of more than one intra-grain diffusion length scale, thus emulating some K-feldspar MDD studies. Similar to most thermochronological studies of alkali feldspar, these four studies used Arrhenius relationships (i.e., younger dates from regions with higher D/r^2) and mathematical cross correlation (C_{fg}; [45]) to test the assumptions that Ar was lost in nature by thermally driven diffusion, and that laboratory degassing revealed natural Ar diffusion kinetics, although these were not verified by petrographic or in situ Ar isotopic analyses.

2.3. Cross Correlation as a Means to Validate MDD Modelling

The use of $^{40}Ar/^{39}Ar$ data and the MDD approach to obtain t-T paths assumes that volume diffusion was the dominant mechanism for the migration of Ar in alkali feldspar and muscovite during their geologic histories and in the laboratory. A further assumption is that Arrhenius relationships obtained at high temperatures and over short timescales in the laboratory are representative of natural degassing at lower temperatures and longer time scales. Some of the approaches to validate these assumptions are straightforward and were cited above. These include, for example, comparisons of the recovered t-T paths with a priori known thermal histories and comparisons of the observed spatial variations of $^{40}Ar/^{39}Ar$ dates with theoretical predictions (e.g., in situ dates becoming younger towards an assumed crystal boundary). However, there is an additional less trivial aspect that is specific for MDD modelling, which is discussed below.

When using the MDD approach, Ar diffusion parameters are determined for a specific sample using an Arrhenius diagram that is constructed from data acquired by step-heating analysis. It is assumed that any departure from linearity in this diagram is due to degassing and mixing of Ar reservoirs from distinct intra-grain diffusion domains that remained stable over geologic and laboratory timescales [4]. Smaller diffusion domains are expected to exhaust early during the analysis, such that the effective radius of diffusion domains that degas gradually increases with progressive heating, as illustrated by the log(r/r0) plot (Figure 1E,F). These smaller domains are expected to have lower closure temperatures, such that the average $^{40}Ar/^{39}Ar$ date of diffusion domains that degas increases with progressive heating (Figure 1A,B). Thus, the topologies of both the log(r/r0) plot and the age spectrum are expected to depend on the distribution of intra-grain diffusion domains. Lovera et al. (2002) [45] developed the normalised cross-correlation coefficient Cfg to quantify the degree of correlation between the log(r/r0) plot and the age spectrum, which is used to validate the assumptions behind MDD theory. They used numerical modelling to show that hypothetical, well-behaved alkali feldspar crystals that comply with all the assumptions behind MDD theory yield highly correlated log (r/r0) plots and age spectra (Cfg > 0.95). On the contrary, crystals whose diffusion domains were fragmented during their synthetic geological past (which was done to simulate fluid-mediated alteration) frequently yielded lower Cfg values (<<0.95), implying that the correlation between the log(r/r0) plots and the age spectrum could be used to check the validity of t-T solutions. Lovera et al. (2002) [45] used these same numerical experiments to argue that only volumetrically significant alteration (>>6 vol%) can substantially reduce the accuracy of t-T paths obtained using the MDD model (in alteration scenarios where Cfg > 0.95).

3. Arguments against the Reconstruction of Continuous t-T Paths Using the $^{40}Ar/^{39}Ar$ Method

The validity of the underlying assumptions and approaches described above to use $^{40}Ar/^{39}Ar$ data from K-feldspar and muscovite to recover t-T information has been challenged in several studies. It has been shown that diffusion profiles can be significantly modified by (i) semi-closed system behaviour, and the introduction of extraneous Ar from grain boundary fluids, which is common in high-pressure phengite (e.g., [18,53]; Figure 2),

and (ii) fluid induced recrystallisation and low temperature alteration (e.g., [16,54–57]). Furthermore, it was also suggested that mechanisms of Ar migration in laboratory diffusion experiments and in nature are not the same, such that laboratory-derived kinetics of Ar release cannot be used in thermochronological modelling (e.g., [14,58]). Finally, it has been proposed that arguments used to validate the assumptions behind MDD modelling are not valid [59]. Here we summarise key evidence and arguments that contest the application of $^{40}Ar/^{39}Ar$ data from K-feldspar and muscovite for thermochronology in its current form (i.e., using both step-heating and in situ techniques).

3.1. The Effects of Fluid Interaction and Closed-System Behaviour

A fundamental observation in nature is that metasomatic fluids are more efficient at mobilizing isotopes than temperature (e.g., [60–65]). Kinetic rate constants for fluid mediated transport of solutes are orders of magnitude larger, with significantly smaller activation energies than thermally driven diffusion (e.g., [66]). Consequently, many authors conclude that Ar redistribution and loss from K-feldspar and white micas in nature is controlled by sub-solidus transformations and/or fluid interaction (e.g., [2,3,12,14,30,54–56,67–71]), and volume diffusion is subordinate.

The misidentification of even minor secondary replacement phases and their Ar isotope reservoirs can lead to significant inaccuracies in t-T paths when using the MDD approach. MDD analysis requires that the activation energy for Ar diffusion is determined, enabling the log(r/r0) plot to be constructed and used to calculate the relative volumes of the discrete domains. This is usually done using heating steps at low degassing temperatures (Figure 1C–F), where gas may be predominately released from alteration phases that are not representative of the primary mineral phase [14]. Consequently, the form of the log(r/r0) plot is extremely sensitive to the presence of those alteration phases.

Argon isotope ratios in K-bearing secondary phases will also be influenced by thermal diffusion, and thus they could be theoretically exploited to derive t-T solutions. Therefore, the identification of secondary phases could provide more temporally resolved thermal history information. However, we envisage extreme difficulty in exploiting these phases as thermochronometers because the user must be able to determine their time of formation, and the accuracy of the t-T paths will be subject to all of the phenomena that are discussed here (Section 3).

3.1.1. Alkali Feldspar

The Chain of Ponds Pluton, USA, and the Aar Massif, Swiss Alps

The MDD model was developed via experiments using alkali feldspar extracted from the Chain of Ponds Pluton, New England [4,5,46,72,73], and the realization that separate samples apparently contained a distribution of domain sizes with respect to thermally driven diffusion of ^{40}Ar. However, with the exception of Fitz Gerald and Harrison (1993) [73], these early pioneering studies did not present a petrological study of the alkali feldspar crystals, and assumed they were not affected by interaction with fluids. However, mineralogical evidence indicates that fluid-induced recrystallisation and alteration are common in alkali feldspar, including in samples used to develop the MDD model [2,12,67,71,74–76].

Chafe et al. (2014) [71] sampled the Chain of Ponds Pluton at the same location where Heizler et al. (1988) [72] took the samples that were first used to develop the MDD model. Their petrographic characterisation of the alkali feldspar crystals (cathodoluminescence, back-scatter electron imaging, and electron-probe microanalysis) showed that primary magmatic alkali feldspars in hand-picked and un-hand-picked (i.e., not screened for visible alteration under a binocular microscope) aliquots had been affected by successive generations of fluid infiltration (Figure 3A), causing adularisation and the introduction of celsian-rich veins. Correlations between K, Ca and Cl that had been directly measured and inferred from the Ar isotopic data showed that degassing of heterochemical phases is responsible for deviations of Arrhenius trajectories from linearity (Figure 3B), as op-

posed to a range in diffusion lengths in an inert, homogeneous medium with a constant absolute diffusivity. Chafe et al. (2014) [71] conclude that alkali feldspar samples should be generally suspected to contain multiple, heterochemical, diachronous generations and that the loss of argon is predominantly an effect of large-scale recrystallization in an open system, which can give rise to staircase-shaped age spectra (Figure 3A). Similarly, Villa and Hanchar (2013) [2] combined petrological characterization with Sr, Pb and Ar isotope analyses to study alkali feldspar from the Aar metagranites, Central Alps, Switzerland. Comparisons of Pb and Sr isotopic compositions, and Ca/K, Cl/K and $^{40}Ar/^{39}Ar$ dates led them to conclude that staircase-shaped age spectra were a result of degassing primary and metasomatic feldspar, with little relation to volume diffusion through geological time.

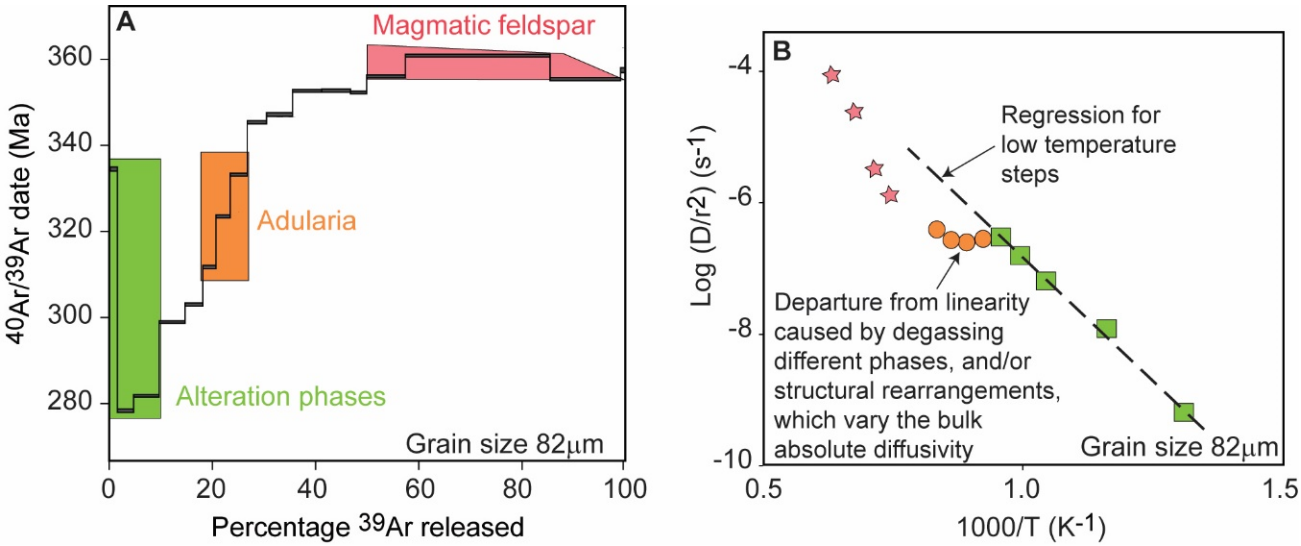

Figure 3. (**A**) Staircase-shaped age spectrum for alkali feldspar extracted from the Chain of Ponds Pluton (New England, USA), highlighting the contribution of gas derived from alteration phases, adularia and pristine magmatic alkali feldspar. The relative contributions suggest the staircase topology is a consequence of the co-existence of heterochemical phases with different apparent ages (data and interpretation from [71]). (**B**) Arrhenius data corresponding to the age spectrum in (**A**), which shows that (i) variations from linearity are due to degassing of different retrogressed phases and variations in diffusivity (D; as opposed to solely being due to variations in diffusion length scale), and (ii) activation energy determinations derived from regressing the low temperature steps (determined from the gradient) relate to alteration phases, and not pristine, magmatic feldspar. Colours relate to the same phases that are labelled in (**A**). Data and graphs are from Chafe et al. (2014) [71]. The inferences about magmatic feldspar, adularia and alteration phases were made by combining EPMA, CL images and the argon isotope data.

Megacrystic Alkali feldspar from Itrongay, Madagascar

Arguably the most convincing evidence that supports alkali feldspar thermochronology using the $^{40}Ar/^{39}Ar$ method was presented in studies of alkali feldspar from Itrongay, Madagascar. Previous studies include Flude et al. (2014) [6], who reported a core to rim $^{40}Ar/^{39}Ar$ date profile that was interpreted to result from diffusive loss of ^{40}Ar (Figure 2A), and the work of Nägler and Villa (2000) [77], who reported $^{40}Ar/^{39}Ar$ and K-Ca dates and suggested the younger $^{40}Ar/^{39}Ar$ date was a consequence of diffusive loss of ^{40}Ar. However, these interpretations were recently questioned by Popov et al. (2020a) [16], who utilised cathodoluminescence and back-scatter electron imaging of a transparent, cm-scale crystal of Itrongay feldspar to reveal at least five distinct zones (Figure 4A–E; [16]) that formed in five distinct episodes of growth from fluids with distinctly different compositions (SiO_2 rich, CO_2 rich, and later H_2O rich). Each zone yields distinguishable weighted mean $^{40}Ar/^{39}Ar$ (in situ) dates that span between 477–176 Ma, while most dates are younger than the K-Ca isochron date of 477 ± 2 Ma ([77]; Figure 4F–H). The spatial coincidence of abrupt in situ $^{40}Ar/^{39}Ar$ dates and crystal zonation strongly suggests the dominant cause

of variation in dates was dissolution-precipitation reactions that collectively span tens to hundreds of millions of years. This is inconsistent with the conclusions of Flude et al. (2014) [6], who without petrographically analyzing their feldspar crystal from Itrongay, interpreted their in situ date profiles to be a consequence of volume diffusion through a continuous crystal structure (Figure 2A), and thus conclude that Itrongay feldspar crystals acted as grain-scale diffusion domains. Popov et al. (2020a) [16] note that some in situ $^{40}Ar/^{39}Ar$ dates of the inner zone (zone 1 in Figure 4A,B) of their crystal increase towards its outer boundary. They hypothesise that ^{40}Ar has diffused into the boundaries that form between the feldspar host and inclusions, and thus older in situ dates are a consequence of ablating regions with higher densities of inclusions, and thus they do not entirely rule out potential experimental evidence for volume diffusion on small scales.

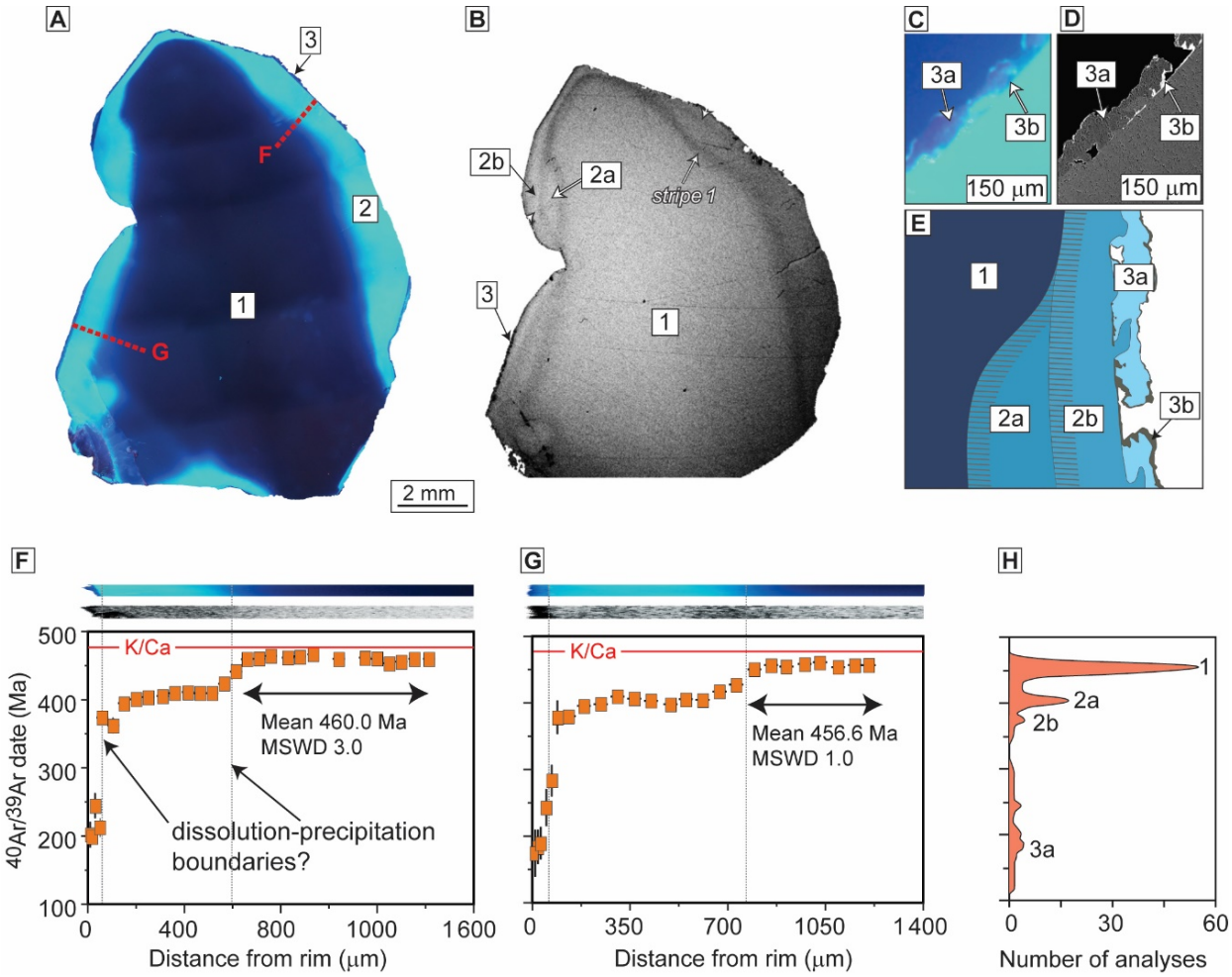

Figure 4. Gem quality orthoclase extracted from pegmatites at the site "Itrongay", southern Madagascar, collected by the authors during field work in 2016. (**A**) Composite optical cathodoluminescence image showing three distinct zones (labeled 1, 2 and 3). (**B**) Back-scatter electron image which shows that zone 2 can be divided into two sub-zones (2a and 2b), which are separated by a dark stripe. (**C**,**D**) cathodoluminescence and back-scatter electron images of the outer ~300 µm of the crystal, which show that zone 3 can be divided into 2 sub-zones (3a, 3b). (**E**) schematic sketch (not to scale) showing the relationships between all zones and their sub-zones. (**F**,**G**) In situ core-rim $^{40}Ar/^{39}Ar$ dates from our own in situ study [16], showing strip maps of back-scatter electron and cathodoluminescence images. Distinguishable variations in $^{40}Ar/^{39}Ar$ dates correspond with crystallographic zones, revealing periods of dissolution and diachroneity in crystallisation (~477–176 Ma). (**H**) Probability density function of all in situ $^{40}Ar/^{39}Ar$ dates collected from 8 traverses into the same crystal shown in (**A**). Detailed petrographic analyses of single crystals question previous interpretations that variations in in situ $^{40}Ar/^{39}Ar$ dates are dominated by volume diffusion. Data and images are from [16].

Klokken Syenite, Greenland

Alkali feldspars from the Klokken syenite (U-Pb baddeleyite age 1166 ± 4 Ma; [78]) have been central to the debate on the natural causes of the distribution of ^{40}Ar in alkali feldspars. Parsons et al. (1988) [67] combined ^{40}Ar/^{39}Ar step-heating and transmission electron microscopy to show that Ar leakage from some alkali feldspar from the Klokken syenite was promoted by the formation of micropores (sub-µm channels) that give rise to a turbid (translucent–opaque) appearance. This microporosity formed by the interaction of deuteric fluids at ~500 °C [76], which remove coherency strain and thus the volume proportion of strain-controlled intergrowths, ultimately forming coarse patch perthites composed of subgrains (e.g., coherent boundaries of perthitic lamellae; [79]). More recent studies [76] showed that later microstructures formed and evolved in the Klokken feldspars between ~450 and less than 90 °C after the formation of the patch perthite, and describe eight feldspar phases in single crystals. Scanning Electron Microscopy showed the youngest and lowest temperature phase contains a K-feldspar end member, with microstructures that are similar to those found in authigenic feldspars.

Parsons et al. (1988) [67] present a systematic relationship between ^{40}Ar/^{39}Ar total fusion dates and feldspar texture. The least affected cryptoperthite yields ^{40}Ar/^{39}Ar dates that are 20–60 Ma younger than their crystallisation age (Figure 5A), while the most turbid feldspars (which host ≤4.5vol% micropores; [80]) yield ^{40}Ar/^{39}Ar step-dates as young as ~400 Ma with total fusion dates that are younger than 1 Ga (Figure 5B; [67,81,82]). Harrison et al. (2010) [70] studied the same crystals that were analysed by Parsons et al. (1988; e.g., crystal 140025; Figure 5C) [67] using high spatial resolution ^{40}K-^{40}Ca dating by secondary ion mass spectrometry. They observed that the ^{40}K-^{40}Ca system was variably disturbed to yield apparent isochrons ranging from 718 to 2400 Ma and suggested that the disturbance occurred at ≤718 Ma, and possibly as late as ~400 Ma. They concur that primary feldspar from the Klokken Syenite has been modified by aqueous fluid mediated modification, and characterisation of mineral textures is paramount before attempting to extract thermal history information.

Clearly, turbid feldspar from Klokken has lost radiogenic ^{40}Ar through geologic time, perhaps by the infiltration of fluids that utilise the micropermeability that micropores can create (e.g., [79,80,82,83]), and also perhaps because the average interatomic bond strengths are weakened by connected pores (e.g. [2]). Furthermore, the observation that the crystals with the finest scale intergrowths are the most retentive to ^{40}Ar is counterintuitive to the MDD model. Overall, these open the possibility that the non-deuterically altered crypto-perthitic phases may have lost some ^{40}Ar by volume diffusion, and their ^{40}Ar/^{39}Ar dates are consistent with being at T < 200 °C since they formed ([82], Sanders, 2008). However, younger ^{40}Ar/^{39}Ar and K/Ca dates from regions characterised by micropores and subgrains suggests that fluid-induced replacement reactions can modify the argon isotopic compositions of alkali feldspars at any time after they form [76,82].

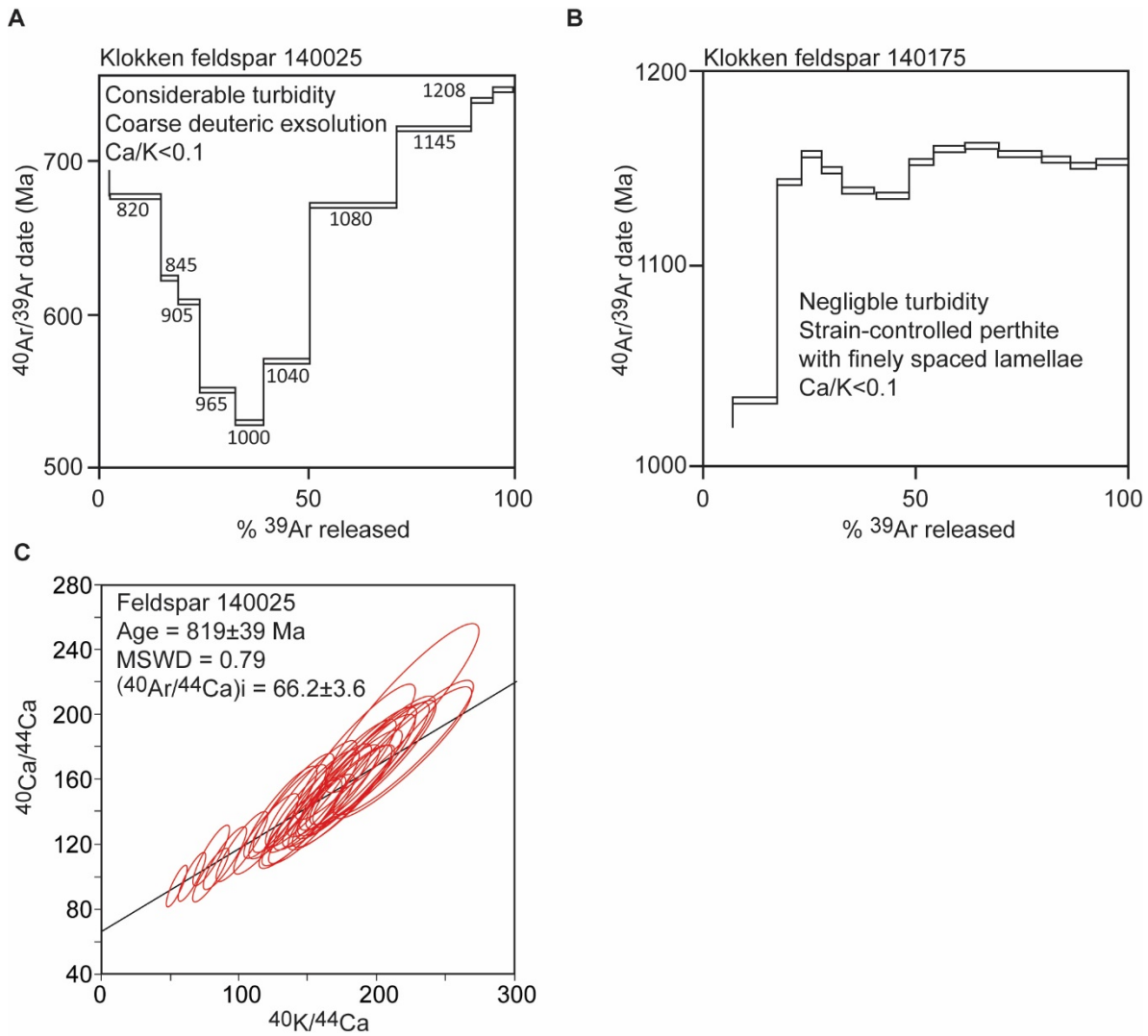

Figure 5. (**A**) Step-heating spectrum for alkali feldspar from sample 140025 of the Klokken layered series, which has considerable turbidity and coarse deuteric alteration, with $^{40}Ar/^{39}Ar$ step dates that are considerably younger than the zircon U-Pb baddeleyite age of the syenite [67]. (**B**) Step-heating spectrum for alkali feldspar from sample 140175 of the Klokken layered series, which is a strain controlled microperthite that lacks turbidity, with a total fusion age (1125 ± 16 Ma) that suggests <5% of ^{40}Ar has been lost [67]. (**C**) K-Ca data for alkali feldspar from sample 140025. The young isochron age relative to the U-Pb baddeleyite age was used by Harrison et al. (2010) [70] to conclude that the Klokken syenite was affected by aqueous fluid-mediated dissolution-reprecipitation, and the $^{40}Ar/^{39}Ar$ data are mainly not a consequence of thermally driven ^{40}Ar loss.

3.1.2. Muscovite

Several studies have demonstrated that fluid interaction and retrogression can alter Ar isotopic compositions in white mica by driving recrystallisation and mica breakdown (e.g., [1,3,53,54,69,84,85]), which occur at much faster rates than thermal isotopic resetting. Consequently, $^{40}Ar/^{39}Ar$ dates of white mica frequently do not reflect the cooling history expected from P-T-t models (via thermal diffusion), and thus are not cooling ages. Forward modelling of Ar diffusion in high-pressure white micas was performed by Warren et al. (2011; phengite in pelites of the Saih Hatah high-pressure terrane, Oman) [86] and McDonald et al. (2016; phengite and muscovite, Western Gneiss Region, Norway) [3], assuming a single diffusion length scale, to show that the distribution of in situ and single crystal fusion dates of high pressure white micas are not compatible with natural diffusion being the dominant mechanism for the redistribution of Ar. Rather, these authors combined electron

probe microanalyses of white micas with single grain and in situ $^{40}Ar/^{39}Ar$ analyses to show that the $^{40}Ar/^{39}Ar$ dates were a result of chemical breakdown, partial melting and fluid ingress (Figure 6A,B). Villa et al. (2019) [56] and Bulle et al. (2020) [57] degassed magmatic and hydrothermal muscovite from the Lardarello-Travale Geothermal Field, Italy, by step-wise heating, and compared Ar isotopic data with K, Cl and Ca abundances obtained by electron microprobe analyses, and in situ $d^{18}O$ measurements to assess the significance of $^{40}Ar/^{39}Ar$ dates. A Cl-poor, magmatic mica (2.7 Ma) and Cl-rich hydrothermal mica (0.7 Ma) are inter-grown at the micron scale (Figure 6C), which gives rise to highly variable $^{40}Ar/^{39}Ar$ ages at km scales, showing that the Ar record in their muscovite samples is dominantly a result of structure-controlled infiltration of meteoric water, and was not caused by ambient temperature and diffusion. Finally, Mulch and Cosca (2004) [1] combined in situ $^{40}Ar/^{39}Ar$ dating, $\delta^{18}O$ determinations and electron probe microanalysis with detailed micro-structural studies to show that variations in $^{40}Ar/^{39}Ar$ dates in syntectonic muscovite fish from the Porsgrunn-Kristiansand Shear Zone (southern Norway) reflect recrystallisation during extensional deformation, and equilibration with meteoric fluids. The most compositionally variable muscovites that consist of recrystallised subgrains yield the largest dispersion in $^{40}Ar/^{39}Ar$ dates, which is not a function of thermally driven diffusion (Figure 6D,E).

Heterogeneous distributions of Ar isotope reservoirs in phengite grains on the cm to sub-mm scale can also be a consequence of grain boundary fluids, either by (i) the introduction of Ar into the grains from Ar-rich fluids, where older ^{40}Ar is derived from an earlier generation of K-bearing minerals (e.g., [18]), or by (ii) inefficient removal of Ar due to restricted grain boundary fluid circulation (e.g., [53,87,88]). Semi-closed system behaviour that retains inherited ^{40}Ar and reduces the efficiency of ^{40}Ar removal is contrary to the assumption that ^{40}Ar diffuses from the grain (or sub-grain domain) to a fully open system, and significantly complicates linking Ar concentrations to thermal histories. For example, Di Vincenzo et al. (2004) [89] suggest that white micas of the Variscan basement of Sardinia did not experience Ar loss during subsequent heating to >500 °C due to the presence of high Ar concentrations at their grain boundaries. Phengite from the Western Gneiss Complex crystallised at <770 °C, with peak metamorphism at 410–400 Ma [90], and diffusion modelling with a fully open system suggests the single grain phengite dates should be ~21–3 Ma younger than the time of crystallisation [53]. On the contrary, in situ $^{40}Ar/^{39}Ar$ dates vary between ~518–389 Ma, implying that grains with dates <400 Ma have lost some Ar. However, Ar may have diffused into the older grains from either the grain boundary fluid, adjacent grains, or have been incorporated as excess ^{40}Ar during crystallisation (Figure 6A). The scattered dates reported by McDonald et al. (2018) [53] preclude the construction of an inverse isochron, and thus cannot easily distinguish between these possibilities. Importantly, semi-closed boundary behaviour does not preclude using the Ar isotope data to obtain t-T paths, although it is included in this review because it significantly complicates the process, and has not yet been accounted for in thermochronological studies.

3.2. Laboratory Degassing and Changes in Diffusivity (D)

A key assumption when numerically simulating diffusion to obtain t-T solutions is that the displacing isotopes utilise the same mineral pathways in the laboratory as they use in nature, i.e., that grains or intra-grain diffusion domains in the material used to obtain diffusion data remain stable over the course of laboratory experiments. In other words, thermochronologists must be cautious when extrapolating laboratory derived diffusion parameters obtained at high temperatures and short time scales to geologically relevant conditions at lower temperatures and longer time scales. Do structural changes occur at temperatures lower than laboratory degassing? Does the acquisition of $^{40}Ar/^{39}Ar$ data by step-heating (i.e., MDD analysis) emulate the mechanisms that drove Ar loss during its geologic past?

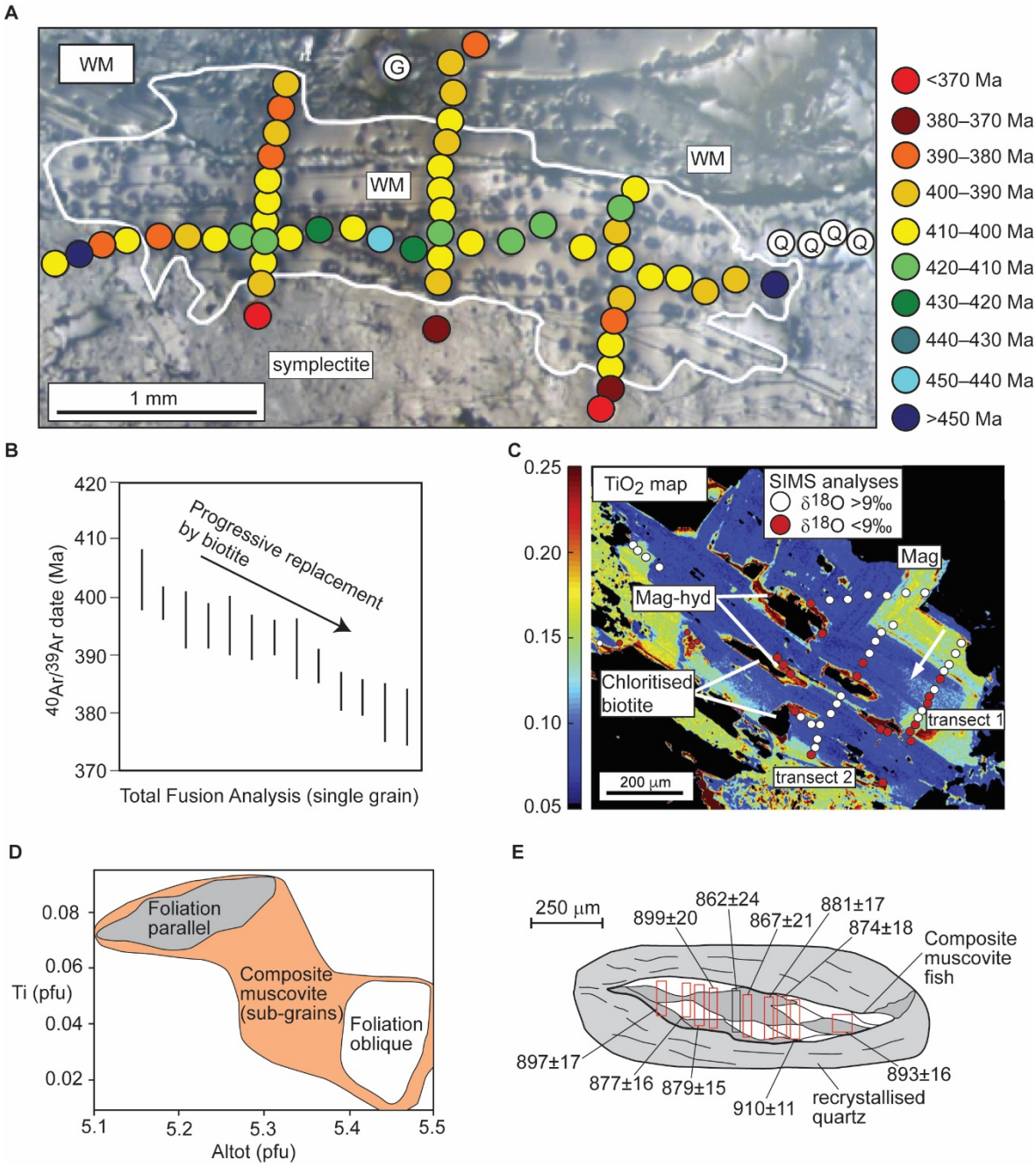

Figure 6. (**A**) In situ $^{40}Ar/^{39}Ar$ dates in white mica in medium grained, unfoliated gneisses, Western Gneiss Complex, Norway [3]. The white mica has been partially replaced at the rims by biotite-plagioclase symplectites. The dates reveal patchy date distributions with no clear core-rim profiles, which would be predicted by volume diffusion with a fully open boundary. Diffusion has not been the sole mechanism that redistributed Ar, despite cooling from temperatures (~700 °C) well above the closure temperature. Rather, Ar distribution was dominated by white mica breakdown to biotite (**B**), and the introduction of extraneous Ar from a semi-closed grain boundary network. G: Garnet, Q: Quartz, WM: White Mica. Data and interpretation are from McDonald et al. (2016) [3]. (**C**) Microscale $d^{18}O$ and chemical variability of muscovite within monzogranite from the Larderello-Travale Geothermal Field (Italy), with a medium grained, typical igneous texture with primary magmatic white mica (mag) that is partially chloritised, hydrothermal white mica (mag-hyd) and late stage sericite (data and images are from [57]). (**D**) Ti and Al compositions of low-Al, foliation parallel (grey) and high-Al, foliation oblique (white) muscovite crystals from the Porsgrunn-Kristiansand Shear Zone, southern Norway [1]. The orange field shows the range of compositions obtained from composite muscovite fish (shown in (**E**)) that cover the entire compositional range, and also yield the largest range in in situ $^{40}Ar/^{39}Ar$ dates. Red rectangles show the region of in situ ablations, and white and dark fields are the same as those shown in (**D**).

To test this, Lovera et al. (1993) [46] conducted a double-irradiation experiment where the same alkali feldspar fragments were step-heated to 850 °C, before and after a second irradiation. Sanders (2008) [82] compared step-heating $^{40}Ar/^{39}Ar$ data derived from several aliquots of three alkali feldspar fractions, where some aliquots were partially outgassed at different temperatures prior to irradiation. Both studies found only a minor effect of laboratory heating on the properties and the size distribution of the hypothetical intragrain diffusion domains over timescales relevant to conventional step-heating analysis. However, it remains unclear as to which features separate these domains from each other and provide fast diffusion pathways for the effective removal of Ar from their surfaces. On the contrary, several experimental observations show that non-linearity in Arrhenius plots is either due to fracturing or opening of fast diffusion pathways during sample preparation [91], fast pathways for Ar loss that modify during progressive step-heating (e.g., [17,30]), or modifications of intrinsic diffusion parameters by heating-induced structural transitions (e.g., [14,58,92]). Regardless, it is critical to understand how the microtextural evolution of minerals during laboratory step-heating affects $^{40}Ar/^{39}Ar$ data, and whether or not laboratory data can be extrapolated to geological temperatures and timescales.

3.2.1. Alkali Feldspar

Ar diffusivity data from alkali feldspar frequently define non-linear arrays in Arrhenius plots. This non-linearity lies at the base of MDD theory, where it is accounted for by the presence of multiple intra-grain diffusion domains that remain stable through laboratory heating to the initiation of melting. Indeed, any Arrhenius plot that can be represented as a monotonic non-decreasing log(r/r0) is consistent with such an explanation. However, this explanation is not unique, and many studies relate the non-linearity to modifications of texture and structure during laboratory heating. Previous suggestions include homogenisation of compositionally different domains within the analysed fragments along with annealing or formation of crystal defects [12,30,93], fracturing of the analysed fragments and the formation of Ar traps within them [17,91,94], structural transitions [71,92,93] and changes in vacancy-specific diffusion mechanisms [34,55].

One group of suggestions about the causes of non-linearity in Arrhenius plots relates it to the instability of boundaries that define apparent intra-grain diffusion domains during diffusion experiments. Detailed mineralogical observations have shown that commonly occurring alkali feldspar has a range of very complex textures on a micro- to nanoscale that are modified due to laboratory heating. For example, approximately 70% (by volume) of alkali feldspar megacrysts from Shap Granite are optically pristine, whereas the remaining regions are turbid (e.g., [29–31]). The pristine regions are magmatic feldspar that exsolved by Na-K interdiffusion to form coherent to semi-coherent Na-rich lamellae in a K-rich matrix. They are transected by nanotunnels that formed by feldspar dissolution into fluids along misfit dislocations at the boundaries of semi-coherent lamellae. The turbid regions are feldspar that formed via fluid-induced dissolution-reprecipitation and include veins of replacement Na-rich and K-rich sub-grains with incoherent boundaries. Most of these textures are unstable during laboratory heating, as was first hypothesised by Parsons et al. (1999) [12] and then experimentally documented by Fitz Gerald et al. (2006) [29], Parsons et al. (2010) [30] and Popov et al. (2020b) [17]. During step-heating, exsolution lamellae in Shap feldspar start to homogenise at ≥500 °C, while complete homogenisation can be achieved at ≥700 °C and the process is complete in less than 1 hr at 1000 °C. Partial homogenisation also occurs between incoherent Na-rich and K-rich sub-grains in replacive veins. Furthermore, upon heating to ≥500 °C nanotunnels disappear or become less obvious, exsolution lamellae get intersected by small cracks and arrays of planar micropores form around them. Heating to >700 °C leads to the formation of abundant subspherical nanopores [30]. Finally, heating results in the development of interconnected cracks, which form due to spatially uneven thermal expansion because of regions with varied chemical composition and state of Si-Al order (Figure 7; [17]). Cracks were also

reported in heated grains of alkali feldspar from the Chain of Ponds Pluton [73], the Klokken intrusion [82], and the Benson Mines pegmatite [94].

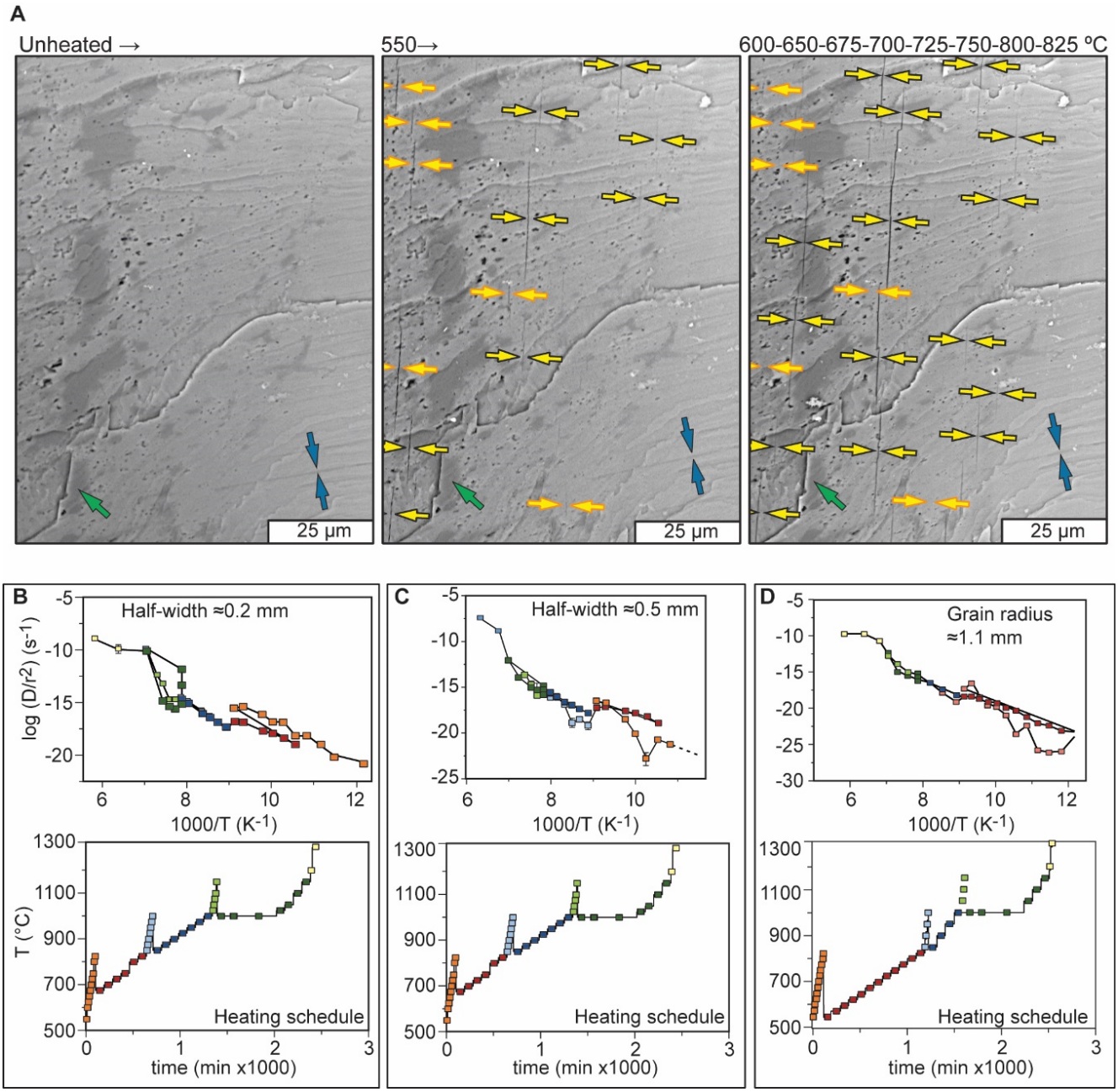

Figure 7. (**A**) Back-scatter electron images of uncoated (010) cleavage surfaces of an alkali feldspar fragment taken from the Shap Granite, UK. The images were taken in the same region before step-heating (left), after a single 10 min heating step at 550 °C (middle) and after an additional eight heating steps at 600–825 °C (right). Blue arrows show exsolution lamellae. Green arrows highlight replacement perthite veins (dark regions are Na-rich, brighter regions are K-rich). Yellow arrows show cracks: black outline indicates cracks that did not disappear with progressive heating, orange outline indicates cracks that appeared after 1 heating step and became invisible after 9 heating steps. (**B**–**D**) Arrhenius plots for the step/heating experiments with the corresponding repetitive heating schedules. The Arrhenius trajectory of smaller grains is consistent with MDD theory, while grains with half widths of 0.5 mm and larger yield smaller values for D/r^2 for higher temperature heating steps, which is contradictory to MDD theory. Non-linearity in the Arrhenius trajectories was ascribed to the evolution of fracturing during step-heating. All data and images are taken from Popov et al. (2020b) [17].

Some authors have suggested that modifications to the texture of alkali feldspar dynamically alter the boundaries of apparent intra-grain diffusion domains [12,29,30,94]. However, until recently these suggestions were not supported by any diffusivity data, which may have led other authors to conclude that changes in alkali feldspar texture incurred during laboratory heating, such as fracturing, play no important role in laboratory degassing [73,82]. However, Popov et al. (2020b) [17] reported Ar diffusivity data showing that the effective diffusion length of alkali feldspar from Shap Granite decreased during progressive step-heating by at least a factor of ~15 in grains that are larger than ~0.5 mm (assuming that E_a and D_0 are unchanged; Figure 7C,D). They related this decrease to fracturing, which was shown to continue with increased heating using electron microscopy observations (Figure 7A). The effective diffusion length appeared to increase with progressive heating in smaller grains, such that their Arrhenius plots were consistent with predictions of the MDD model (Figure 7B). This was interpreted by Popov et al. (2020b) [17] to be due to the greater chance of cracks that form early in the step-heating process intersecting the grain surface. Clearly, any attempt to reconcile curved Arrhenius trajectories with the MDD model must first verify that the proposed intra-grain diffusion domains remain stable during laboratory heating.

Another group of suggestions about the cause of non-linearity in Arrhenius plots focuses on time and/or temperature dependent changes in parameters that characterise Ar diffusion through the alkali feldspar structure (i.e., E_a and D_0). Some authors speculate that non-linearity may be caused by changes in vacancy-specific diffusion mechanisms [34,55,94]. Foland (1994) [94] also suggested that radiation damage can attenuate Ar diffusion and its annealing during step-heating can complicate Ar release. While these ideas were not developed further, evidence from diffusion studies in other materials [95–98] shows that there is potential for such phenomena to occur in alkali feldspar. Cassata and Renne (2013) [92] utilised molecular dynamics considerations to suggest that the downward curvature of Arrhenius trajectories of sodic feldspars and potassic feldspars with exsolved Na-rich lamellae is due to changes in the rate of thermal expansion during a transition from triclinic to monoclinic symmetry. They supported this idea using step-heating experiments with anorthoclase aliquots with different sizes from Easy Chair Crater, USA (and other feldspars), which yielded non-linear Arrhenius arrays for Ar outgassing at temperatures near the triclinic-monoclinic transition and linear Arrhenius arrays for Ne outgassing at much lower temperatures. The claim was made that following MDD theory, these arrays require that smaller grain fragments have smaller sized domains, which led those authors to conclude that the non-linear Arrhenius trajectories must be caused by changes in diffusivity. However, as pointed out by Lovera et al., (2015) [99], these arrays can be explained within the framework of MDD theory if the largest domain is assumed to occupy most of the analysed fragment (see also [17]). Finally, Kung and Villa (2021) [58] observed that the rate of Ar release from a cleavage fragment of orthoclase from Itrongay, Madagascar, varied during laboratory degassing at a constant temperature of 888 ± 2 °C (Figure 8A), which they correlated with heating-induced changes in vibrational modes documented by Raman spectroscopy. However, most of the changes in vibrational modes were instantaneous and reversible, and thus it is unclear how they can affect Ar diffusion. Perhaps more importantly, Kung and Villa (2021) [58] observed an irreversible change of colour, indicating that the inventory of structure defects had changed, and they also report that the degassed fragment "crumbled into dozens of euhedral cleavage fragments", suggesting that many cracks had formed. The importance of the latter is corroborated by the log(r/r0) plot (Figure 8B), which can be interpreted as showing a decrease of the effective diffusion length until ~30% of ^{39}Ar was released.

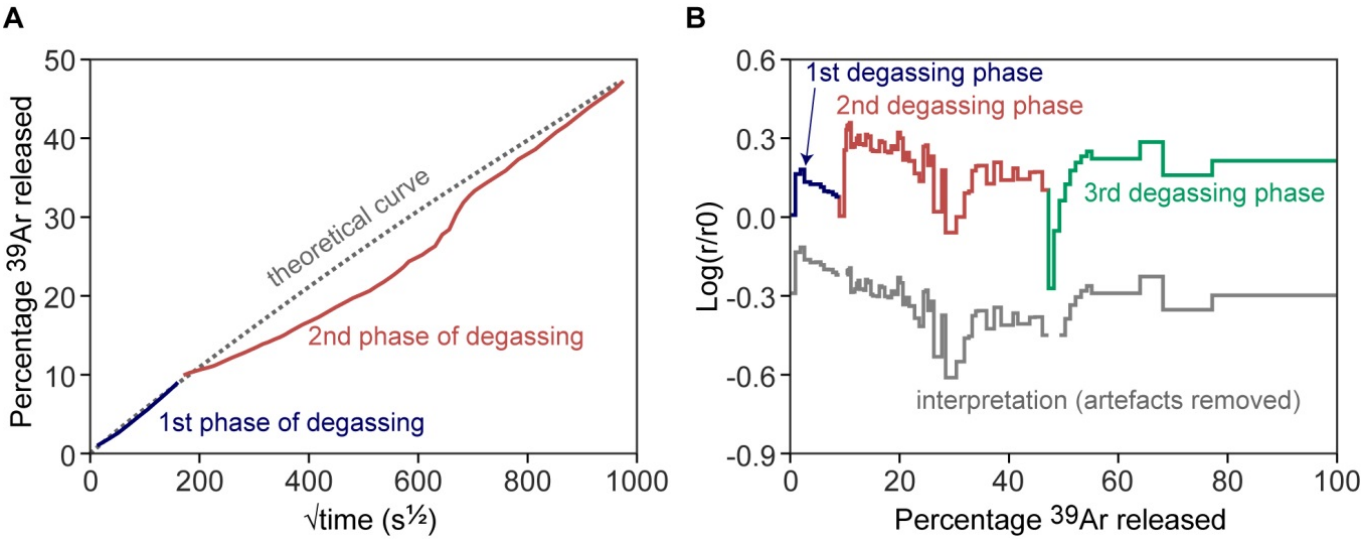

Figure 8. Data from Kung and Villa (2021) [58] obtained by in-vacuo degassing of alkali feldspar from Itrongay, Madagascar. The experiment included 3 heating phases where the 1st and 2nd phases were heated at 888 °C, while the 3rd phase was step-heated between 1024 °C and 1449 °C. The analysed fragment was removed from the spectrometer between each heating phase. (**A**) ^{39}Ar degassing rates during the first 2 phases of heating compared to a theoretical curve for a single domain with constant diffusivity (see [58], for details). The departure of the experimental from the theoretical curve was interpreted to reflect changes in diffusivity through time. (**B**) log(r/r0) plot for all 3 heating phases assuming an activation energy of 241.9 kJ/mol (derived from the slope defined by heating steps 76 and 77). The topology of the log(r/r0) plot for the first 2 phases of heating does not depend on the activation energy because the heating temperature remained constant. Abrupt changes in log(r/r0) coincide with reloading of the analysed fragment into the spectrometer and thus may represent an analytical artifact. We have attempted to correct for these artifacts (grey line) by (i) arbitrarily shifting the plot segment of the 1st phase of heating by −0.3 log units (to avoid overlap with the original data, rendering it easier to see), and (ii) shifting the plot segments of the 2nd and 3rd phases of heating such that the second heating step in each of them yields the same log(r/r0) value as the final heating step in the preceding phase of heating. Note that the effective diffusion length decreases until ~30% of ^{39}Ar has been released, after which it increases. This trend in log(r/r0) is visible in the log(r/r0) plot with and without artefacts, and is consistent with observation that the heated fragment crumbled into dozens of euhedral cleavage fragments after the 2nd phase of heating [58].

Summarising, many authors argued that heating-induced structural modifications affect the diffusion of Ar in alkali feldspar during laboratory experiments. While unambiguous evidence to support these claims is currently lacking, existing data warrant more careful consideration of whether Ar diffusivity data obtained in the laboratory at higher temperatures can be extrapolated to lower temperatures to model Ar diffusion over geological timescales. The latter is important for both step-heating and in situ approaches to ^{40}Ar/^{39}Ar thermochronology because both approaches use laboratory derived diffusion parameters.

3.2.2. Muscovite

Unlike alkali feldspar, muscovite micas are hydrous, and it has been known for some time that dehydration reactions during step-wise degassing of Ar can cause micas that have an a priori known zoned intra-grain Ar distribution to yield plateaus on age spectra [100]. This is generally unsurprising because degassing hydrous muscovite in vacuo proceeds by structural modifications during dehydroxylation that start at ~650–780 °C [101–103]. Dehydroxylated muscovite has cell parameters that are larger than hydrated muscovite [104], and thus it seems possible that diffusivities also vary with structural expansion (e.g., see [92]).

Célèrier (2007) [105] and Harrison et al. (2009) [7] examined the Ar loss characteristics in muscovite during hydrothermal heating experiments, and conclude that vacuum degassing of both hydrothermally treated, and in vacuo step-heating of muscovite can

be described by a diffusion model with multiple diffusion length scales, and thus that dehydroxylated muscovite preserves $^{40}Ar/^{39}Ar$ gradients that can be subsequently used to obtain thermal history solutions using the MDD approach. Since then, some $^{40}Ar/^{39}Ar$ age gradients in age spectra have been interpreted as diffusion gradients, and have been used to estimate the diffusivities of discrete domains with the general assumption that only primary igneous phases were degassing and that these remained stable throughout the degassing experiment (e.g., [10,11,106]). In response, Villa (2021) [107] recently re-examined the data of Célèrier (2007) [105] in detail, and based on the study of Hess et al. (1987) [108] suggest that a more highly resolved analysis of the muscovites using TEM would probably reveal reaction products, which are the cause of staircase-shaped age spectra. This would be consistent with the observation by Harrison et al. (2009) [7] who report fine, euhedral neoformed grains that crystallised during hydrothermal heating. Villa (2021) [107] concludes that the range of variations in Ca/K ratios in muscovite can only be accounted for by open system reactions (and possibly the neoformed grains observed by Harrison et al., 2009; [7]) during the hydrothermal degassing experiments, and volume diffusion has not dominated Ar loss.

3.3. Relevance of Cross-Correlation of log(r/r0) Plots with Age Spectra

Lovera et al. (2002) [45] used numerical modelling of fluid-mediated recrystallisation to show that log(r/r0) plots and age spectra are expected to be highly correlated if Ar loss during laboratory heating occurred along the same boundaries and via the same mechanism as in the geologic past. According to them, the frequent observation of high correlations (>70% of samples in their database) simultaneously validates the assumption that natural ^{40}Ar loss was dominated by volume diffusion and that sample-specific Ar diffusivity data acquired by step-heating can be used to obtain accurate t-T paths by inversion modelling. However, fluid-mediated recrystallisation of alkali feldspar simulated by Lovera et al. (2002) [45] only caused fragmentation of intra-grain diffusion domains, leaving volume diffusion as the sole mechanism for ^{40}Ar displacement. A more realistic approach to simulating the effects of fluid interaction was taken by Popov and Spikings (2020; Figure 9) [59], where ^{40}Ar is completely removed from the affected zones at the time of fluid interaction, mimicking the consequence of fluid-induced dissolution-reprecipitation (e.g., [55,71,109]). They showed that the age spectrum and log(r/r0) plots can also be highly correlated when fluid flow affects Ar loss through geological time, and dry volume diffusion drives degassing in the laboratory. This correlation exists because fluid-mediated alteration can also lead larger domains to have generally older apparent $^{40}Ar/^{39}Ar$ dates, which is a prediction of MDD theory. Furthermore, the same simulations also showed that volumetrically low degrees of recrystallisation and alteration (e.g., ~3%) can significantly reduce the accuracy of t-T solutions constructed using MDD theory. Therefore, high Cfg values alone cannot be used to validate the assumptions behind MDD theory and the accuracy of its predicted thermal histories.

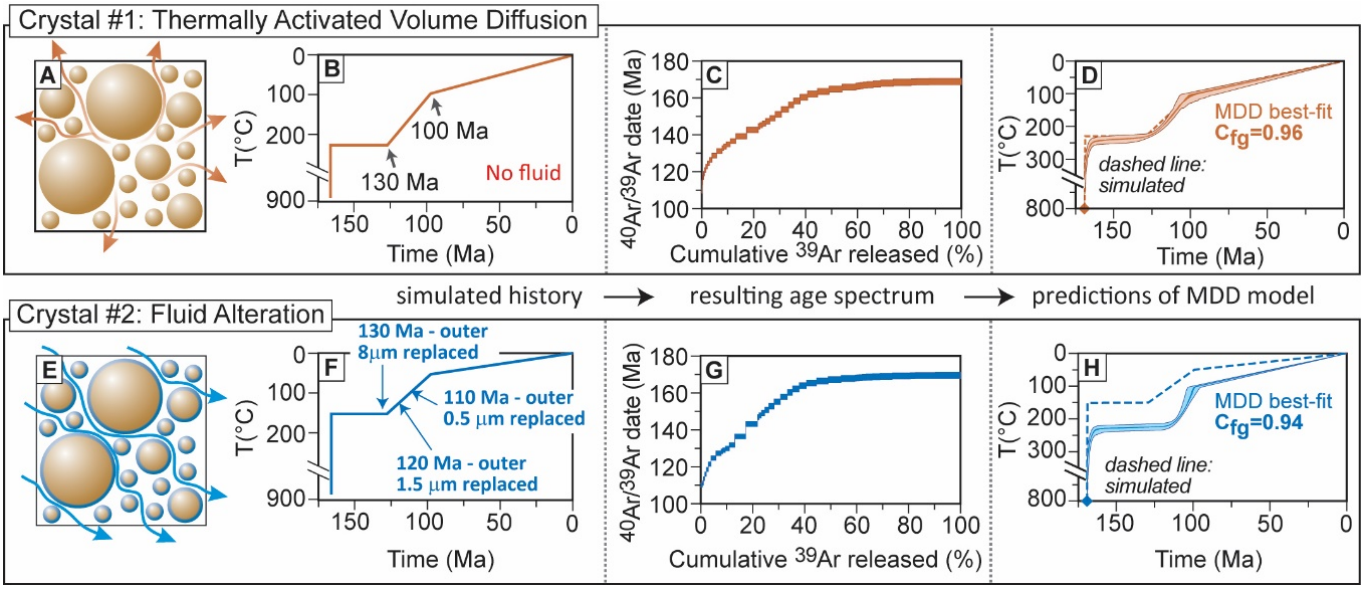

Figure 9. Forward modelling of Popov and Spikings (2020) [59] to test the ability of the Cfg parameter (Lovera et al., 2002) to compare laboratory and natural Ar degassing mechanisms, and thus the validity of MDD inversion to generate accurate t-T histories. All simulations assume that laboratory degassing occurs by volume diffusion, and only the mode of natural Ar loss is modified. (**A**–**D**) no fluid interaction during natural degassing; (**E**–**H**) fluid interaction driving dissolution-precipitation and Ar loss. Figures show forward modelled t-T paths and aqueous history (**B**,**F**), resultant age spectra (**C**,**G**) and best-fit t-T solutions generated by inversion using MDD modelling (**D**,**H**). In scenario with no fluid interaction a crystal with 3 non-interacting spherical domains with radii of 150, 50 and 16 microns occurring in proportions 1:5:150 have only lost ^{40}Ar by volume diffusion. The best fit t-T path obtained by MDD inversion yields a high degree of correlation (crystal #1; Cfg = 0.96) between the age spectrum and the log(r/ro) plot (not shown), and the modelled t-T path obtained by MDD inversion (**D**) closely matches the original t-T path (**B**). Similarly, we forward modelled a t-T path (**F**) with accompanying fluid assisted dissolution-precipitation that reset specific volumes of the three modelled domains at specific times (crystal #2). The best fit t-T path obtained by MDD inversion yields a Cfg of 0.94, although the t-T solution (**H**) does not accurately recreate the original t-T model (**F**). MDD theory would utilise the high degree of correlation to interpret the t-T paths obtained by MDD inversion in both cases, as accurate. Details are provided in Popov and Spikings (2020) [59].

4. Recommendations

Displacement of isotopes by volume diffusion always occurs, although it is unlikely to displace isotopes at rates that dominate over the effects of fluid-induced modifications. Potassium-rich alkali feldspars from magmatic rocks are normally a combination of semi-coherent perthite with one or more replacement phases, and thus it is likely that multiple phases of replacement are commonplace in plutonic feldspars [75,76]. Therefore, while studies of alkali feldspar from the Chain of Ponds Pluton, Aar Massif, Klokken Syenite and Itrongay may not entirely negate the application of diffusion theory to recover t-T paths, they reveal the paramount importance of combining a detailed textural study of single crystals with ^{40}Ar/^{39}Ar data before doing so. A similar conclusion can be made regarding white micas, where a combination of petrology and in situ ^{40}Ar/^{39}Ar dates of white mica from high pressure terranes in Oman, the Western Gneiss region and Porsgrunn-Kristiansand Shear Zone in Norway, and the Lardarello-Travale Geothermal Field in Italy clearly reveal the absolute necessity of first accounting for fluid interaction and secondary reaction products before seeking diffusion profiles and extracting t-T information. In addition, an expanding database of experimental evidence shows that laboratory step-heating at elevated temperatures (e.g., ~400–1100 °C) can induce structural and textural changes such as symmetry transitions, dehydroxylation, and creation and annealing of crystal structure defects and cracking, and thus extreme caution must be made when extrapolating laboratory derived rate loss constants (D/r^2) to the geologic past. However, some publications that have combined in situ ^{40}Ar/^{39}Ar dates with petrological information could not

rule out the possibility of the presence of diffusion profiles on small scales. Thus, it may be possible to use such data to find crystals of alkali feldspar and white mica that are suitable for thermochronology, and below we provide some recommendations that will assist in the recovery of potential t-T paths.

(1) Even carefully selected grains of alkali feldspar and muscovite from common magmatic and metamorphic rocks are likely to represent polycrystalline materials featuring multiple generations of a single or several minerals. Therefore, it is of paramount importance to characterise such grains prior to isotopic analysis to identify the likely causes of disturbances in $^{40}Ar/^{39}Ar$ systematics. At bare minimum, thermochronological interpretations of $^{40}Ar/^{39}Ar$ data should be supported by cathodoluminescence and/or high-contrast back scattered electron images. Chemical and isotope composition can provide further evidence for the presence of recrystallised regions as well as their origin. Of particular importance are Ca, K and Cl, as they partially convert to Ar isotopes during neutron irradiation and provide information on the sources of the analysed gas. Attention should be paid even to volumetrically minor secondary alteration. For example, the study of [59] Popov and Spikings (2020) showed that only 3–6 vol% of reprecipitated K-rich feldspar can significantly change t-T paths obtained by the MDD approach. $^{40}Ar/^{39}Ar$ dates of Muscovite are frequently older than from K-feldspar in the same rock sample (e.g., [39]), which is predicted by thermal-diffusion, although this does not negate the possibility that fluid interaction has modified the Ar isotopic composition.

(2) In vacuo step-heating for the purposes of thermochronology should only be performed on grains where any intra-grain diffusion domains are shown to be stable and any non-linearity in Arrhenius relationships for Ar diffusivity through an uninterrupted structure is known and can be accounted for. The applicability of extrapolation of experimentally determined diffusion parameters to geological temperatures and time scales should be carefully assessed. In vacuo step-heating degassing experiments can be affected by phenomena such as heating-induced fracturing, symmetry changes, the appearance and disappearance of various structure defects, and dehydroxylation. Hydrothermal degassing experiments can be influenced by mineral reactions whereby the rate constants of degassing compound several displacement mechanisms, and include Ar loss via mineral reactions as well as diffusive loss. Therefore, detailed observations are required to assess the degree of mineral transformation when extracting parameters for Ar diffusion from both types of experimental data (step-heating and in situ ablation). Cross correlation of age spectra and log(r/r0) plots should not be used to compare laboratory and natural degassing pathways because high-degrees of cross-correlation can also be achieved when these are not equivalent.

(3) In situ analyses are extremely powerful because they can directly associate $^{40}Ar/^{39}Ar$ dates with textural and compositional information, and thus can be used to seek what may at least be suspect diffusion profiles from what is shown to be regions that formed at the same time and have equivalent intrinsic diffusion properties. Such regions in alkali feldspars may include regions that are distal from any later veins, or regions within homogeneous cores of gem-like megacrystic feldspars (e.g., Itrongay feldspar). However, the extraction of thermal history information from such profiles is dependent on knowledge of the intrinsic diffusion properties (see recommendation ii), which cannot be obtained from in situ data without an apriori knowledge of the thermal history. Furthermore, as with the step-heating approach, the in situ technique also requires an understanding of the boundary condition, where the concentration of Ar isotopes may only be semi-closed (see Popov and Spikings, this issue). Numerous in situ dates are required from any given monomineralic phase to attempt to recover the composition of the non-radiogenic isotope reservoir(s).

(4) Overall, the $^{40}Ar/^{39}Ar$ technique has tremendous potential to reveal information about fluid flow, deformation, the timing of sub-solidus transformations and thermal histories. It is likely that in most cases $^{40}Ar/^{39}Ar$ dates neither record end-member fluid events nor thermal diffusion profiles, and are instead mixed dates. However, extracting

the thermal-diffusion component requires careful petrographic analyses with elemental and isotopic characterisation, which are the primary tools to deduce the origins of the Ar isotope reservoirs. Arguably, with the exception of $^{40}Ar/^{39}Ar$ geochronology of sanidine from volcanic rocks, $^{40}Ar/^{39}Ar$ data are better used to estimate the timing of fluid flow and deformation events (i.e., the age of neo-formed grains).

Author Contributions: Conceptualization: R.A.S., investigation, R.A.S. and D.V.P.; data curation, R.A.S. and D.V.P.; writing—original draft preparation, R.A.S. and D.V.P.; writing—review and editing, R.A.S., funding acquisition, R.A.S. and D.V.P. Both authors have read and agreed to the published version of the manuscript.

Funding: This review benefited from funding from the Swiss National Science Foundation grants 200021_160052, awarded to R.A.S., and an Early Postdoctoral Mobility fellowship P2GEP2_191478, awarded to D.V.P.

Data Availability Statement: This is a review, and therefore all data can be found indexed from the original sources in the citations that are provided.

Acknowledgments: The manuscript benefited from discussions with members of the Isotope Geochemistry group at the University of Geneva.

Conflicts of Interest: The authors declare no conflict of interest. The funders had no role in the design of the study, in the collection, analyses, or interpretation of data, in the writing of the manuscript, or in the decision to publish the results.

References

1. Mulch, A.; Cosca, M.A. Recrystallization or Cooling Ages: In Situ UV-Laser $^{40}Ar/^{39}Ar$ Geochronology of Muscovite in Mylonitic Rocks. *J. Geol. Soc.* **2004**, *161*, 573–582. [CrossRef]
2. Villa, I.M.; Hanchar, J.M. K-Feldspar Hygrochronology. *Geochim. Cosmochim. Acta* **2013**, *101*, 24–33. [CrossRef]
3. McDonald, C.S.; Warren, C.J.; Mark, D.F.; Halton, A.M.; Kelley, S.P.; Sherlock, S.C. Argon Redistribution during a Metamorphic Cycle: Consequences for Determining Cooling Rates. *Chem. Geol.* **2016**, *443*, 182–197. [CrossRef]
4. Lovera, O.M.; Richter, F.M.; Harrison, T.M. The $^{40}Ar/^{39}Ar$ Thermochronometry for Slowly Cooled Samples Having a Distribution of Diffusion Domain Sizes. *J. Geophys. Res.* **1989**, *94*, 17917. [CrossRef]
5. Lovera, O.M.; Richter, F.M.; Harrison, T.M. Diffusion Domains Determined by ^{39}Ar Released during Step Heating. *J. Geophys. Res.* **1991**, *96*, 2057. [CrossRef]
6. Flude, S.; Halton, A.M.; Kelley, S.P.; Sherlock, S.C.; Schwanethal, J.; Wilkinson, C.M. Observation of Centimetre-Scale Argon Diffusion in Alkali Feldspars: Implications for $^{40}Ar/^{39}Ar$ Thermochronology. *Geol. Soc. Lond. Spec. Publ.* **2014**, *378*, 265–275. [CrossRef]
7. Harrison, T.M.; Célérier, J.; Aikman, A.B.; Hermann, J.; Heizler, M.T. Diffusion of ^{40}Ar in Muscovite. *Geochim. Cosmochim. Acta* **2009**, *73*, 1039–1051. [CrossRef]
8. Warren, C.J.; Hanke, F.; Kelley, S.P. When Can Muscovite $^{40}Ar/^{39}Ar$ Dating Constrain the Timing of Metamorphic Exhumation? *Chem. Geol.* **2012**, *291*, 79–86. [CrossRef]
9. Forster, M.A.; Lister, G.S. $^{40}Ar/^{39}Ar$ Geochronology and the Diffusion of ^{39}Ar in Phengite–Muscovite Intergrowths during Step-Heating Experiments *in Vacuo*. *Geol. Soc. Lond. Spec. Publ.* **2014**, *378*, 117–135. [CrossRef]
10. Long, S.P.; Heizler, M.T.; Thomson, S.N.; Reiners, P.W.; Fryxell, J.E. Rapid Oligocene to Early Miocene Extension Along the Grant Range Detachment System, Nevada, USA: Insights From Multipart Cooling Histories of Footwall Rocks. *Tectonics* **2018**, *37*, 4752–4779. [CrossRef]
11. Gonzalez, J.P.; Baldwin, S.L. Modelling White Mica Pressure-temperature-time (P-T-t) Paths Using Thermobarometric and $^{40}Ar/^{39}Ar$ Thermochronologic Data. *Terra Nova* **2019**, *31*, 169–178. [CrossRef]
12. Parsons, I.; Brown, W.L.; Smith, J.V. 40 Ar/ 39 Ar Thermochronology Using Alkali Feldspars: Real Thermal History or Mathematical Mirage of Microtexture? *Contrib. Mineral. Petrol.* **1999**, *136*, 92–110. [CrossRef]
13. Di Vincenzo, G.; Ghiribelli, B.; Giorgetti, G.; Palmeri, R. Evidence of a Close Link between Petrology and Isotope Records: Constraints from SEM, EMP, TEM and in Situ ^{40}Ar–^{39}Ar Laser Analyses on Multiple Generations of White Micas (Lanterman Range, Antarctica). *Earth Planet. Sci. Lett.* **2001**, *192*, 389–405. [CrossRef]
14. Villa, I.M. Diffusion of Ar in K-Feldspar: Present and Absent. *Geol. Soc. Lond. Spec. Publ.* **2014**, *378*, 107–116. [CrossRef]
15. Uunk, B.; Brouwer, F.; ter Voorde, M.; Wijbrans, J. Understanding Phengite Argon Closure Using Single Grain Fusion Age Distributions in the Cycladic Blueschist Unit on Syros, Greece. *Earth Planet. Sci. Lett.* **2018**, *484*, 192–203. [CrossRef]
16. Popov, D.V.; Spikings, R.A.; Scaillet, S.; O'Sullivan, G.; Chew, D.; Badenszki, E.; Daly, J.S.; Razakamanana, T.; Davies, J.H.F.L. Diffusion and Fluid Interaction in Itrongay Pegmatite (Madagascar): Evidence from in Situ $^{40}Ar/^{39}Ar$ Dating of Gem-Quality Alkali Feldspar and U Pb Dating of Protogenetic Apatite Inclusions. *Chem. Geol.* **2020**, *556*, 119841. [CrossRef]

17. Popov, D.V.; Spikings, R.A.; Kouzmanov, K. Pathways for ^{39}Ar Loss during Step-Heating of Alkali Feldspar Megacrysts from the Shap Granite (UK): Combined Evidence from Diffusion Experiments and Characterisation of Heating-Induced Texture Modifications. *Chem. Geol.* **2020**, *547*, 119677. [CrossRef]
18. Scaillet, S. Excess ^{40}Ar Transport Scale and Mechanism in High-Pressure Phengites: A Case Study from an Eclogitized Metabasite of the Dora-Maira Nappe, Western Alps. *Geochim. Cosmochim. Acta* **1996**, *60*, 1075–1090. [CrossRef]
19. Camacho, A.; Lee, J.K.W.; Hensen, B.J.; Braun, J. Short-Lived Orogenic Cycles and the Eclogitization of Cold Crust by Spasmodic Hot Fluids. *Nature* **2005**, *435*, 1191–1196. [CrossRef]
20. Popov, D.V.; Spikings, R.A. Numerical Modelling of Radiogenic Ingrowth and Diffusion of Pb in Apatite Inclusions with Variable Shape and U-Th Zonation. *Minerals* **2021**, *11*, 364. [CrossRef]
21. Lovera, O.M. Computer Programs to Model ^{40}Ar/^{39}Ar Diffusion Data from Multidomain Samples. *Comput. Geosci.* **1992**, *18*, 789–813. [CrossRef]
22. Zeitler, P.K. Inversion of ^{40}Ar/^{39}Ar Age Spectra Using the Controlled-Random-Search Method. *EOS* **1993**, *74*, 650.
23. Lister, G.S.; Baldwin, S.L. Modelling the Effect of Arbitrary P-T-t Histories on Argon Diffusion in Minerals Using the MacArgon Program for the Apple Macintosh. *Tectonophysics* **1996**, *253*, 83–109. [CrossRef]
24. Pickles, C.S.; Kelley, S.P.; Reddy, S.M.; Wheeler, J. Determination of High Spatial Resolution Argon Isotope Variations in Metamorphic Biotites. *Geochim. Cosmochim. Acta* **1997**, *61*, 3809–3833. [CrossRef]
25. Skipton, D.R.; Schneider, D.A.; Kellett, D.A.; Joyce, N.L. Deciphering the Paleoproterozoic Cooling History of the Northeastern Trans-Hudson Orogen, Baffin Island (Canada), Using ^{40}Ar/^{39}Ar Step-Heating and UV Laser Thermochronology. *Lithos* **2017**, *284–285*, 69–90. [CrossRef]
26. Skipton, D.R.; Warren, C.J.; Hanke, F. Numerical Models of P–T, Time and Grain-Size Controls on Ar Diffusion in Biotite: An Aide to Interpreting ^{40}Ar/^{39}Ar Ages. *Chem. Geol.* **2018**, *496*, 14–24. [CrossRef]
27. Wheeler, J. Diffarg: A Program for Simulating Argon Diffusion Profiles in Minerals. *Comput. Geosci.* **1996**, *22*, 919–929. [CrossRef]
28. Baxter, E.F. Quantification of the Factors Controlling the Presence of Excess 40 Ar or 4 He. *Earth Planet. Sci. Lett.* **2003**, *216*, 619–634. [CrossRef]
29. Fitz Gerald, J.D.; Parsons, I.; Cayzer, N. Nanotunnels and Pull-Aparts: Defects of Exsolution Lamellae in Alkali Feldspars. *Am. Mineral.* **2006**, *91*, 772–783. [CrossRef]
30. Parsons, I.; Fitz Gerald, J.D.; Lee, J.K.W.; Ivanic, T.; Golla-Schindler, U. Time–Temperature Evolution of Microtextures and Contained Fluids in a Plutonic Alkali Feldspar during Heating. *Contrib. Mineral. Petrol.* **2010**, *160*, 155–180. [CrossRef]
31. Lee, J.K.W. Multipath Diffusion in Geochronology. *Contrib. Mineral. Petrol.* **1995**, *120*, 60–82. [CrossRef]
32. Harrison, T.M.; Lovera, O.M. The Multi-Diffusion Domain Model: Past, Present and Future. *Geol. Soc. Lond. Spec. Publ.* **2014**, *378*, 91–106. [CrossRef]
33. Richter, F.M.; Lovera, O.M.; Mark Harrison, T.; Copeland, P. Tibetan Tectonics from ^{40}Ar/^{39}Ar Analysis of a Single K-Feldspar Sample. *Earth Planet. Sci. Lett.* **1991**, *105*, 266–278. [CrossRef]
34. Wartho, J.-A.; Kelley, S.P.; Brooker, R.A.; Carroll, M.R.; Villa, I.M.; Lee, M.R. Direct Measurement of Ar Diffusion Profiles in a Gem-Quality Madagascar K-Feldspar Using the Ultra-Violet Laser Ablation Microprobe (UVLAMP). *Earth Planet. Sci. Lett.* **1999**, *170*, 141–153. [CrossRef]
35. Copeland, P.; Mark Harrison, T.; Le Fort, P. Age and Cooling History of the Manaslu Granite: Implications for Himalayan Tectonics. *J. Volcanol. Geother. Res.* **1990**, *44*, 33–50. [CrossRef]
36. Arnaud, N.O.; Brunel, M.; Cantagrel, J.M.; Tapponnier, P. High Cooling and Denudation Rates at Kongur Shan, Eastern Pamir (Xinjiang, China) Revealed by ^{40}Ar/^{39}Ar Alkali Feldspar Thermochronology. *Tectonics* **1993**, *12*, 1335–1346. [CrossRef]
37. Kirby, E.; Reiners, P.W.; Krol, M.A.; Whipple, K.X.; Hodges, K.V.; Farley, K.A.; Tang, W.; Chen, Z. Late Cenozoic Evolution of the Eastern Margin of the Tibetan Plateau: Inferences from ^{40}Ar/^{39}Ar and (U-Th)/He Thermochronology: Late cenozoic evolution of eastern tibet. *Tectonics* **2002**, *21*, 1001. [CrossRef]
38. Metcalf, J.R.; Fitzgerald, P.G.; Baldwin, S.L.; Muñoz, J.-A. Thermochronology of a Convergent Orogen: Constraints on the Timing of Thrust Faulting and Subsequent Exhumation of the Maladeta Pluton in the Central Pyrenean Axial Zone. *Earth Planet. Sci. Lett.* **2009**, *287*, 488–503. [CrossRef]
39. Spikings, R.A.; Foster, D.A.; Kohn, B.P.; Lister, G.S. Post-Orogenic (<1500 Ma) Thermal History of the Palaeo-Mesoproterozoic, Mt. Isa Province, NE Australia. *Tectonophysics* **2002**, *349*, 327–365. [CrossRef]
40. McDannell, K.T.; Schneider, D.A.; Zeitler, P.K.; O'Sullivan, P.B.; Issler, D.R. Reconstructing Deep-time Histories from Integrated Thermochronology: An Example from Southern Baffin Island, Canada. *Terra Nova* **2019**, *31*, 189–204. [CrossRef]
41. Foster, D.A.; John, B.E. Quantifying Tectonic Exhumation in an Extensional Orogen with Thermochronology: Examples from the Southern Basin and Range Province. *Geol. Soc. Lond. Spec. Publ.* **1999**, *154*, 343–364. [CrossRef]
42. Wong, M.S.; Gans, P.B.; Scheier, J. The ^{40}Ar/^{39}Ar Thermochronology of Core Complexes and Other Basement Rocks in Sonora, Mexico: Implications for Cenozoic Tectonic Evolution of Northwestern Mexico. *J. Geophys. Res.* **2010**, *115*, B07414. [CrossRef]
43. Dunlap, W.J.; Fossen, H. Early Paleozoic Orogenic Collapse, Tectonic Stability, and Late Paleozoic Continental Rifting Revealed through Thermochronology of K-Feldspars, Southern Norway. *Tectonics* **1998**, *17*, 604–620. [CrossRef]
44. Lovera, O.M.; Harrison, T.M.; Grove, M. Comment on "Multipath Ar Transport in K-Feldspar Deduced from Isothermal Heating Experiments" by Igor Villa. *Earth Planet. Sci. Lett.* **1996**, *140*, 281–283. [CrossRef]

45. Lovera, O.M.; Grove, M.; Harrison, T.M. Systematic Analysis of K-Feldspar 40 Ar/ 39 Ar Step Heating Results II: Relevance of Laboratory Argon Diffusion Properties to Nature. *Geochim. Cosmochim. Acta* **2002**, *66*, 1237–1255. [CrossRef]
46. Lovera, O.M.; Heizler, M.T.; Harrison, T.M. Argon Diffusion Domains in K-Feldspar II: Kinetic Properties of MH-10. *Contrib. Mineral. Petrol.* **1993**, *113*, 381–393. [CrossRef]
47. Hames, W.E.; Hodges, K.V. Laser ^{40}Ar/^{39}Ar Evaluation of Slow Cooling and Episodic Loss of ^{40}Ar from a Sample of Polymetamorphic Muscovite. *Science* **1993**, *261*, 1721–1723. [CrossRef]
48. Scharf, A.; Handy, M.R.; Schmid, S.M.; Favaro, S.; Sudo, M.; Schuster, R.; Hammerschmidt, K. Grain-Size Effects on the Closure Temperature of White Mica in a Crustal-Scale Extensional Shear Zone—Implications of in-Situ ^{40}Ar/^{39}Ar Laser-Ablation of White Mica for Dating Shearing and Cooling (Tauern Window, Eastern Alps). *Tectonophysics* **2016**, *674*, 210–226. [CrossRef]
49. Baldwin, S.L.; Harrison, T.M. Geochronology of Blueschists from West-Central Baja California and the Timing of Uplift in Subduction Complexes. *J. Geol.* **1989**, *97*, 149–163. [CrossRef]
50. Heizler, M.; Ralser, S.; Karlstrom, K.E. Late Proterozoic (Grenville?) Deformation in Central New Mexico Determined from Single-Crystal Muscovite ^{40}Ar/^{39}Ar Age Spectra. *Precambrian Res.* **1997**, *84*, 1–15. [CrossRef]
51. Heizler, M.T.; Harrison, T.M. Continuous Thermal Histories from Muscovite ^{40}Ar/^{39}Ar Age Spectra. *Geochim. Cosmochim. Acta* **2009**, *73* , A497.
52. Forster, M.A.; White, L.T.; Ahmad, T. Thermal History of a Pebble in the Indus Molasse at the Margin of a Himalayan Metamorphic Core Complex. *J. Virt. Ex.* **2011**, *38*, 1–21. [CrossRef]
53. McDonald, C.S.; Regis, D.; Warren, C.J.; Kelley, S.P.; Sherlock, S.C. Recycling Argon through Metamorphic Reactions: The Record in Symplectites. *Lithos* **2018**, *300–301*, 200–211. [CrossRef]
54. Villa, I.M. Isotopic Closure. *Terra Nova* **1998**, *10*, 42–47. [CrossRef]
55. Villa, I.M. From Nanometer to Megameter: Isotopes, Atomic-Scale Processes, and Continent-Scale Tectonic Models. *Lithos* **2006**, *87*, 155–173. [CrossRef]
56. Villa, I.M.; Bulle, F.; Rubatto, D.; Ruggieri, G.; Luisier, C.; Baumgartner, L.P. *The Oxygen-Argon Connection in Micas from a Long-Lived Hydrothermal System, Larderello-Travale Geothermal Field, Italy*; American Geophysical Union: Washington, DC, USA, 2019; Volume V34A-03.
57. Bulle, F.; Rubatto, D.; Ruggieri, G.; Luisier, C.; Villa, I.M.; Baumgartner, L. Episodic Hydrothermal Alteration Recorded by Microscale Oxygen Isotope Analysis of White Mica in the Larderello-Travale Geothermal Field, Italy. *Chem. Geol.* **2020**, *532*, 119288. [CrossRef]
58. Kung, J.; Villa, I.M. The in Vacuo Release of Ar from Minerals: 2. The Role of Structural Modifications of K-Feldspar during Heating Revealed by Raman Microprobe Analyses. *Chem. Geol.* **2021**, *580*, 120382. [CrossRef]
59. Popov, D.V.; Spikings, R.A. Diffusion vs. Fluid Alteration in Alkali Feldspar ^{40}Ar/^{39}Ar Thermochronology: Does Cross-Correlation of Log(r/R0) and Age Spectra Validate Thermal Histories? *Chem. Geol.* **2020**, *539*, 119506. [CrossRef]
60. Lasaga, A.C. Chapter 7. The atomistic basis of kinetics: Defects in minerals. In *Kinetics of Geochemical Processes*; Lasaga, A.C., Kirkpatrick, J., Eds.; De Gruyter: Berlin, Germany, 1981; pp. 261–320, ISBN 978-1-5015-0823-3.
61. Glodny, J.; Austrheim, H.; Molina, J.F.; Rusin, A.I.; Seward, D. Rb/Sr Record of Fluid-Rock Interaction in Eclogites: The Marun-Keu Complex, Polar Urals, Russia. *Geochim. Cosmochim. Acta* **2003**, *67*, 4353–4371. [CrossRef]
62. Geochronology: Linking the isotopic record with petrology and textures. In *Geochronology: Linking the Isotopic Record with Petrology and Textures*; Vance, D., Müller, W., Villa, I.M., Geological Society of London, Eds.; Geological Society special publication; Geological Society: London, UK, 2003; ISBN 978-1-86239-146-8.
63. Putnis, A. Mineral Replacement Reactions. *Rev. Mineral. Geochem.* **2009**, *70*, 87–124. [CrossRef]
64. Villa, I.M. Diffusion in Mineral Geochronometers: Present and Absent. *Chem. Geol.* **2016**, *420*, 1–10. [CrossRef]
65. Akker, I.V.; Berger, A.; Zwingmann, H.; Todd, A.; Schrank, C.E.; Jones, M.W.M.; Kewish, C.M.; Schmid, T.C.; Herwegh, M. Structural and Chemical Resetting Processes in White Mica and Their Effect on K-Ar Data during Low Temperature Metamorphism. *Tectonophysics* **2021**, *800*, 228708. [CrossRef]
66. Cole, D.R.; Ohmoto, H.; Lasaga, A.C. Isotopic Exchange in Mineral-Fluid Systems. I. Theoretical Evaluation of Oxygen Isotopic Exchange Accompanying Surface Reactions and Diffusion. *Geochim. Cosmochim. Acta* **1983**, *47*, 1681–1693. [CrossRef]
67. Parsons, I.; Rex, D.C.; Guise, P.; Halliday, A.N. Argon-Loss by Alkali Feldspars. *Geochim. Cosmochim. Acta* **1988**, *52*, 1097–1112. [CrossRef]
68. Reddy, S.M.; Potts, G.J.; Kelley, S.P.; Arnaud, N.O. The Effects of Deformation-Induced Microstructures on Intragrain ^{40}Ar/^{39}Ar Ages in Potassium Feldspar. *Geology* **1999**, *27*, 363–366. [CrossRef]
69. Challandes, N.; Marquer, D.; Villa, I.M. P-T-t Modelling, Fluid Circulation, and ^{39}Ar-^{40}Ar and Rb-Sr Mica Ages in the Aar Massif Shear Zones (Swiss Alps). *Swiss J. Geosci.* **2008**, *101*, 269–288. [CrossRef]
70. Harrison, T.M.; Heizler, M.T.; McKeegan, K.D.; Schmitt, A.K. In Situ 40K–40Ca 'Double-plus' SIMS Dating Resolves Klokken Feldspar 40K–^{40}Ar Paradox. *Earth Planet. Sci. Lett.* **2010**, *299*, 426–433. [CrossRef]
71. Chafe, A.N.; Villa, I.M.; Hanchar, J.M.; Wirth, R. A Re-Examination of Petrogenesis and ^{40}Ar/^{39}Ar Systematics in the Chain of Ponds K-Feldspar: "Diffusion Domain" Archetype versus Polyphase Hygrochronology. *Contrib. Mineral. Petrol.* **2014**, *167*, 1010. [CrossRef]
72. Heizler, M.T.; Lux, D.R.; Decker, E.R. The Age and Cooling History of the Chain of Ponds and Big Island Pond Plutons and the Spider Lake Granite, West-Central Maine and Quebec. *Am. J. Sci.* **1988**, *288*, 925–952. [CrossRef]

73. Fitz Gerald, J.D.; Harrison, T.M. Argon Diffusion Domains in K-Feldspar I: Microstructures in MH-10. *Contrib. Mineral. Petrol.* **1993**, *113*, 367–380. [CrossRef]
74. Lee, M.R.; Parsons, I. Dislocation Formation and Albitization in Alkali Feldspars from the Shap Granite. *Am. Mineral.* **1997**, *82*, 557–570. [CrossRef]
75. Parsons, I.; Lee, M.R. Minerals are not just chemical compounds. *Can. Mineral.* **2005**, *43*, 1959–1992. [CrossRef]
76. Parsons, I.; Fitz Gerald, J.D.; Heizler, M.T.; Heizler, L.L.; Ivanic, T.; Lee, M.R. Eight-Phase Alkali Feldspars: Low-Temperature Cryptoperthite, Peristerite and Multiple Replacement Reactions in the Klokken Intrusion. *Contrib. Mineral. Petrol.* **2013**, *165*, 931–960. [CrossRef]
77. Nägler, T.F.; Villa, I.M. In Pursuit of the 40K Branching Ratios: K-Ca and ^{39}Ar–^{40}Ar Dating of Gem Silicates. *Chem. Geol.* **2000**, *169*, 5–16. [CrossRef]
78. Harper, C.L. *On the Nature of Time in Cosmological Perspective*; University of Oxford: Oxford, UK, 1988.
79. Walker, F.D.L.; Lee, M.R.; Parsons, I. Micropores and Micropermeable Texture in Alkali Feldspars: Geochemical and Geophysical Implications. *Mineral. Mag.* **1995**, *59*, 505–534. [CrossRef]
80. Worden, R.H.; Walker, F.D.L.; Parsons, I.; Brown, W.L. Development of Microporosity, Diffusion Channels and Deuteric Coarsening in Perthitic Alkali Feldspars. *Contrib. Mineral. Petrol.* **1990**, *104*, 507–515. [CrossRef]
81. McLaren, S.; Dunlap, W.J.; Powell, R. Understanding K-Feldspar ^{40}Ar/^{39}Ar Data: Reconciling Models, Methods and Microtextures. *J. Geol. Soc.* **2007**, *164*, 941–944. [CrossRef]
82. Sanders, S. K-Feldspar Thermochronology of Proterozoic Basement Rocks: Reconciling Regional Tectonism, Fluid Alteration, and Argon Transport in Microtexturally Complex Feldspar. Ph.D. Thesis, New Mexico Institute of Mining and Technology, Socorro, NM, USA, 2008.
83. Burgess, R.; Kelley, S.P.; Parsons, I.; Walker, F.D.L.; Worden, R.H. ^{40}Ar^{39}Ar Analysis of Perthite Microtextures and Fluid Inclusions in Alkali Feldspars from the Klokken Syenite, South Greenland. *Earth Planet. Sci. Lett.* **1992**, *109*, 147–167. [CrossRef]
84. Hames, W.E.; Cheney, J.T. On the Loss of from Muscovite during Polymetamorphism. *Geochim. Cosmochim. Acta* **1997**, *61*, 3863–3872. [CrossRef]
85. Allaz, J.; Engi, M.; Berger, A.; Villa, I.M. The Effects of Retrograde Reactions and of Diffusion on ^{40}Ar–^{39}Ar Ages of Micas. *J. Petrol.* **2011**, *52*, 691–716. [CrossRef]
86. Warren, C.J.; Sherlock, S.C.; Kelley, S.P. Interpreting High-Pressure Phengite ^{40}Ar/^{39}Ar Laserprobe Ages: An Example from Saih Hatat, NE Oman. *Contrib. Mineral. Petrol.* **2011**, *161*, 991–1009. [CrossRef]
87. Warren, C.J.; Kelley, S.P.; Sherlock, S.C.; McDonald, C.S. Metamorphic Rocks Seek Meaningful Cooling Rate: Interpreting ^{40}Ar/^{39}Ar Ages in an Exhumed Ultra-High Pressure Terrane. *Lithos* **2012**, *155*, 30–48. [CrossRef]
88. Warren, C.J.; Smye, A.J.; Kelley, S.P.; Sherlock, S.C. Using White Mica ^{40}Ar/^{39}Ar Data as a Tracer for Fluid Flow and Permeability under High-*P* Conditions: Tauern Window, Eastern Alps. *J. Metamorph. Geol.* **2012**, *30*, 63–80. [CrossRef]
89. Di Vincenzo, G. The Relationship between Tectono-Metamorphic Evolution and Argon Isotope Records in White Mica: Constraints from in Situ ^{40}Ar-^{39}Ar Laser Analysis of the Variscan Basement of Sardinia. *J. Petrol.* **2004**, *45*, 1013–1043. [CrossRef]
90. Young, D.J.; Kylander-Clark, A.R.C. Does Continental Crust Transform during Eclogite Facies Metamorphism? *J. Meta. Geol.* **2015**, *33*, 331–357. [CrossRef]
91. Arnaud, N.O.; Kelley, S.P. Argon Behaviour in Gem-Quality Orthoclase from Madagascar: Experiments and Some Consequences for Geochronology. *Geochim. Cosmochim. Acta* **1997**, *61*, 3227–3255. [CrossRef]
92. Cassata, W.S.; Renne, P.R. Systematic Variations of Argon Diffusion in Feldspars and Implications for Thermochronometry. *Geochim. Cosmochim. Acta* **2013**, *112*, 251–287. [CrossRef]
93. Evernden, J.F.; Curtis, G.H.; Kistler, R.W.; Obradovich, J.D. Argon Diffusion in Glauconite, Microcline, Sanidine, Leucite and Phlogopite. *Am. J. Sci.* **1960**, *258*, 583–604. [CrossRef]
94. Foland, K.A. Argon Diffusion in Feldspars. In *Feldspars and Their Reactions*; Parsons, I., Ed.; Springer: Dordrecht, The Netherlands, 1994; pp. 415–447, ISBN 978-94-010-4483-7.
95. Schmeling, P. Influence of Radiation Damage upon the Diffusion of Argon in Potassium Chloride. *Phys. Stat. Solid (b)* **1965**, *11*, 175–184. [CrossRef]
96. Saad, A.; Velichko, O.I.; Shaman, Y.P.; Mazanik, A.V.; Fedotov, A.K.; Fedotova, V.V. Modeling of Hydrogen Diffusion in Silicon Crystals. *Nuclear Instrum. Methods Phys. Res. Sect. B Beam Interact. Mater. Atoms* **2006**, *253*, 118–121. [CrossRef]
97. Dohmen, R.; Kasemann, S.A.; Coogan, L.; Chakraborty, S. Diffusion of Li in Olivine. Part I: Experimental Observations and a Multi Species Diffusion Model. *Geochim. Cosmochim. Acta* **2010**, *74*, 274–292. [CrossRef]
98. Gerin, C.; Gautheron, C.; Oliviero, E.; Bachelet, C.; Mbongo Djimbi, D.; Seydoux-Guillaume, A.-M.; Tassan-Got, L.; Sarda, P.; Roques, J.; Garrido, F. Influence of Vacancy Damage on He Diffusion in Apatite, Investigated at Atomic to Mineralogical Scales. *Geochim. Cosmochim. Acta* **2017**, *197*, 87–103. [CrossRef]
99. Lovera, O.M.; Harrison, T.M.; Boehnke, P. Comment on "Systematic Variations of Argon Diffusion in Feldspars and Implications for Thermochronometry" by Cassata and Renne. *Geochim. Cosmochim. Acta* **2015**, *151*, 168–171. [CrossRef]
100. Hodges, K.V.; Harries, W.E.; Bowring, S.A. ^{40}Ar/^{39}Ar Age Gradients in Micas from a High-Temperature-Low-Pressure Metamorphic Terrain: Evidence for Very Slow Cooling and Implications for the Interpretation of Age Spectra. *Geology* **1994**, *22*, 55–58. [CrossRef]

101. Udagawa, S.; Urabe, K.; Hasu, H. The Crystal Structure of Muscovite Dehydroxylate. *J. Jpn. Assoc. Min. Petr. Econ. Geol.* **1974**, *69*, 381–389. [CrossRef]
102. Tokiwai, K.; Nakashima, S. Dehydration Kinetics of Muscovite by in Situ Infrared Microspectroscopy. *Phys. Chem. Miner.* **2010**, *37*, 91–101. [CrossRef]
103. Heller-Kallai, L.; Lapides, I. Dehydroxylation of Muscovite: Study of Quenched Samples. *Phys. Chem. Miner.* **2015**, *42*, 835–845. [CrossRef]
104. Gemmi, M.; Merlini, M.; Pavese, A.; Curetti, N. Thermal Expansion and Dehydroxylation of Phengite Micas. *Phys. Chem. Miner.* **2008**, *35*, 367–379. [CrossRef]
105. Celerier, J. The Structural and Thermal Evolution of the Kumaon and Garwhal (Sic) Lesser Himalaya, India. Ph.D. Thesis, Australian National University, Canberra, Australia, 2007.
106. Kula, J.; Spell, T.L. Recovery of Muscovite Age Gradients by $^{40}Ar/^{39}Ar$ Vacuum Furnace Step-Heating Analysis. *Chem. Geol.* **2012**, *304–305*, 166–174. [CrossRef]
107. Villa, I.M. The in Vacuo Release of Ar from Minerals: 1. Hydrous Minerals. *Chem. Geol.* **2021**, *564*, 120076. [CrossRef]
108. Hess, J.C.; Lippolt, H.J.; Wirth, R. Interpretation of Biotites: Evidence from Hydrothermal Degassing Experiments and TEM Studies. *Chem. Geol. Isotope Geosci. Sect.* **1987**, *66*, 137–149. [CrossRef]
109. Kelley, S. Excess Argon in K–Ar and Ar–Ar Geochronology. *Chem. Geol.* **2002**, *188*, 1–22. [CrossRef]